

The authors would like to thank Anonymous Referee #1 for their constructive comments. Below are our responses.

**Page 3 line 54-55: I disagree with this statement. Many European WRF-Chem modelling evaluation studies have been published in the last few years.**

We have added additional citations of papers that apply WRF-Chem over Europe. However, in our view, studies that focus on evaluation over the whole European domain are still limited to date. If there are particular studies that fulfill this criteria that are not being discussed in the manuscript, the authors would appreciate it if the referee would mention the papers specifically. The sentences in question have been updated as follows to improve clarity: *“The use of WRF-Chem over Europe has increased in recent years (e.g., Forkel et al., 2012; Žabkar et al., 2015; Solazzo et al., 2012a, b; Tuccella et al., 2012; Zhang et al., 2013a, b). However, only a limited number of these studies are dedicated to the evaluation of WRF-Chem-simulated meteorology and chemistry over the whole European domain.”*

**Page 10 line 293-295: Please, in order to prove that differences between the two meteorological simulations are negligible provide statistical indexes or a comparison figure in the supplementary material.**

A table and figures showing the meteorology from the RADM2 simulation has been added to the supplementary material; see Table S1 and Figures S4-S7. Furthermore, the manuscript has been updated as follows to directly address this question.

*“Differences in predicted meteorology between the MOZART and RADM2 simulations are small, with differences in MSLP less than one hundredth of 1%, and differences in T2, WS10, and WD10 generally far below 1%. Since the simulations were run without aerosol-radiative feedbacks, it was expected that the two simulations would show minimal differences in meteorology, and we conclude that differences in O3 and NOx predicted in the MOZART and RADM2 simulations (Section 4.2) are a direct result of differences in the chemistry, rather than chemistry-radiative feedbacks. Statistics for meteorology for the RADM2 simulation can be found in the Supplementary Material, Table S1 and Figures S4-S7.”*

**Page 15 line 478: to be in line with the NOx (NO2 and NO) treatment in MOZART simulation, I suggest to briefly explore NO concentrations in RADM2**

A discussion of NO concentrations in RADM2 has been added to the revised manuscript.

*“Like for MOZART, NO for RADM2 is underpredicted throughout the domain, with NO concentrations slightly more negatively biased than in MOZART in all seasons except Fall, when NO concentrations are higher for RADM2 than for MOZART and show better agreement with the observations. Temporal correlation for NO2 and NO in RADM2 is also found to show similar behavior to the MOZART simulation.”*

**Figure 1: I suggest to represent temperature using the International System unit (K) here and everywhere else in the text.**

The authors prefer to keep temperature in units of Celsius. Although it is not the SI unit, Celsius is widely used in the meteorological community, and is also used in GMD publications (see, e.g.,

<http://www.geosci-model-dev.net/9/1959/2016/gmd-9-1959-2016.pdf>). Furthermore, when calculating relative bias statistics (MB, NMB, MFB) for temperature as in Table 4, using Kelvin rather than Celsius makes the denominator extremely large and the bias extremely small, making relative bias statistics less meaningful. However, if the editor agrees that the temperature unit should be changed to Kelvin, we will make these changes to our manuscript.



The authors would like to thank Anonymous Referee #2 for their constructive comments. Below are our responses.

**1) lines 50-52: The authors give here three examples of air quality models but maybe they could also refer here to the review article of Baklanov et al. (2014) for the online coupled regional meteorology chemistry models in Europe.**

The original manuscript did include a citation to Baklanov et al. 2014 (line 53-54). However, we have added in the revised manuscript a more detailed reference to this manuscript: *"The application of online coupled regional meteorology chemistry models in Europe, among them WRF-Chem, has been recently reviewed by Baklanov et al. [2014]."*

**2) lines 62-64: The importance of time variant chemical boundary conditions for simulated near surface ozone over Europe has been also highlighted in other recent regional modelling studies (see e.g. Akritidis et al., 2013).**

Following the referee's suggestion, the manuscript has been extended, mentioning the importance of temporally varying chemical boundary conditions.

*"The importance of temporally varying chemical boundary conditions in air quality modeling has also been stressed in other studies (including Akritidis et al., 2013; Andersson et al., 2015)."*

**3) line 264: Please provide some more information on the selection of the AirBase stations classified as rural background. Do you include stations with class 1–3 according to the Joly-Peuch classification methodology for surface ozone (Joly and Peuch, 2012). This approach has been also applied in a recent study by Katragkou et al. (2015) for the evaluation of MACC reanalysis near-surface ozone over Europe.**

We used the classification of stations provided with the metadata in AirBase. This is now indicated in the revised manuscript in Section 3.2.2.

*"Because of the relatively coarse horizontal resolution in this model study, model output is only compared against AirBase stations that are classified as "rural background." The station classification was taken from the metadata provided by the EEA for AirBase."*

**4) line 283: You may add one sentence with information for the use and value of SOMO35 index.**

A brief discussion of the purpose and use of the SOMO35 metric has been added to the manuscript in Section 3.3.

*"SOMO35 is an indicator of cumulative annual ozone exposure used in health impact assessments. The accumulated health impact is assumed to be proportional to the sum of concentrations above a cutoff of 35 ppb, chosen because the relationship between O3 and adverse effects is very uncertain below this threshold (WHO, 2013)."*

**5) Looking the Figures 4 and 9 I am wondering why at the lateral boundaries there are such differences between the two simulations with the different chemical mechanisms (RADM2 and MOZART) even though they are constrained with identical O<sub>3</sub> chemical lateral boundary conditions.**

The importance of ozone import into the model domain from the lateral boundary conditions depends not only the concentration at the lateral boundary conditions (as the reviewer notes, in the case of MOZART and RADM2 simulations, these concentrations are the same), but also on the dominant wind flows at the edge of the domain. A plot of seasonally averaged wind vectors from ERA-Interim for 2007, which are the fields used to force model meteorology at the edges of our domain, has been added to the Supplementary Material (Figure S2). The dominant flow of air onto the European continent is from the west, and we see that the western (particularly northwestern) edge of the domain is where seasonally-averaged O<sub>3</sub> values are most similar between the MOZART and RADM2 simulations. At the northwestern edges of the domain, we see that seasonal average O<sub>3</sub> predicted by RADM2 is generally not more than 5% lower than that predicted by MOZART. At the southern and eastern edges of the domain, there is not a strong flow of air into the model domain, which dampens the impact of ozone boundary conditions in this area.

In addition to the addition of Figure S2 to the Supplementary Material, we have made the following addition to the text in Section 4.2.1.

*“Absolute O<sub>3</sub> concentrations are most similar (i.e., less than 5% different) between the mechanisms near the northwest edges of the domain (see Figures 4 and 9), where the prevailing westerly winds (Supplementary Material, Figure S2) mean that O<sub>3</sub> imported from the boundary conditions plays a dominant role.”*

**6) lines 546-551: Normally with NO<sub>x</sub> titration we mean the first order removal process of O<sub>3</sub> through direct reaction with NO which takes place during nighttime and in the vicinity of large NO emission sources. However the presented results refer to summer daytime and maybe this behaviour is related to the saturated NO<sub>x</sub> conditions (or VOC sensitive conditions) in these areas (which is a different issue). The split between NO<sub>x</sub>saturated or NO<sub>x</sub>-sensitive regimes is driven by the chemistry of odd hydrogen radicals with HNO<sub>3</sub> being the dominant sink in the first case and peroxides the dominant sink in the second case. Maybe the authors could also plot the photochemical regimes in their simulations for the month of July using VOC/NO<sub>x</sub> or H<sub>2</sub>O<sub>2</sub>/NO<sub>y</sub> ratios (see also the study of Beekmann and Vautard, ACP, 2010).**

The reviewer is correct; in this discussion the term "NO<sub>x</sub> titration behavior" has been replaced with "NO<sub>x</sub> saturated behavior." Regarding plotting chemical indicators for chemical regime, an additional plot showing the indicator CH<sub>2</sub>O/NO<sub>y</sub> has been added to the Supplementary Material (Figure S12); a brief discussion of this figure is now included in Section 4.3. A comparison of our results on NO<sub>x</sub> vs. VOC sensitivity to the findings of Beekman and Vautard (2010) has also been added to the discussion. The revised discussion is copied below.

*“Notably, the U.K., Benelux, northern France and Paris, and northwest Germany show NO<sub>x</sub>-saturated behavior, in which increased NO<sub>x</sub> emissions lead to decreased O<sub>3</sub> concentrations. NO<sub>x</sub>-saturated regimes*

are also seen around the area of the Mediterranean between Monaco, Genoa and Corsica. An alternate approach to identify areas of  $\text{NO}_x$ -sensitive vs.  $\text{NO}_x$ -saturated regimes is to use indicator ratios (in the base simulation) following Sillman (1995). We have applied this approach with the indicator ratio  $\text{CH}_2\text{O}/\text{NO}_y$  (Figure S12) and find that areas identified as  $\text{NO}_x$  sensitive using the indicator ratio are the same as those identified using the simulation with +30%  $\text{NO}_x$  emissions. These results are also consistent with the areas of Europe found to be  $\text{NO}_x$  saturated in the model study of Beekmann and Vautard (2010). Magnitudes of the observed change in  $\text{O}_3$  in response to increased  $\text{NO}_x$  emissions are quite similar for both mechanisms, although RADM2 shows slightly stronger  $\text{NO}_x$  saturation (i.e., a stronger decrease in  $\text{O}_3$  given a 30% increase in  $\text{NO}_x$  emissions) in the area centered around Benelux, and stronger  $\text{NO}_x$  sensitivity over Scandinavia and northwest Russia.”

**7) lines 558-559: Mind also that the highest sensitivity for ozone production with regards to VOC is at the regions of high  $\text{NO}_x$  emissions as someone would expect for the regions in the VOC limited regime.**

We see that in areas with high  $\text{NO}_x$  emissions such as Benelux, northern France and Germany, and shipping tracks in the Mediterranean, both RADM2 and MOZART predict VOC-sensitive conditions. This point have been added to the discussion in the revised manuscript. However, the increases in  $\text{O}_3$  with +30% VOC emissions are still relatively small. The text has been updated as follows:

*“Areas where MOZART and RADM2 are in agreement in predicting VOC sensitivity (increased  $\text{O}_3$  concentrations in response to increased VOC emissions) are generally those with high  $\text{NO}_x$  emissions, where one would expect the highest VOC sensitivity based on theory; these areas include Benelux, northern France, northwest Germany, and shipping tracks in the Mediterranean. However, the increase in  $\text{O}_3$  concentration is modest for both mechanisms; for RADM2 it is generally limited to increases of 2-4% over the base simulation.”*

**8) lines 565-566: Do you think that the different  $\text{O}_3$  sensitivity to VOC changes in the two schemes can account for the  $\text{O}_3$  differences between RADM2 and MOZART (e.g. the lower ozone values in MOZART)? If yes, in which sense?**

The results of the +30% VOC sensitivity studies for July (Figure 16) indicate that  $d[\text{O}_3]/d[\text{VOC}]$  is higher (more positive) for RADM2 than for MOZART for the chemical regime represented by the models in July 2007. This is an indication that the two mechanisms are simulating different  $\text{O}_3$  chemical regimes – in the case of RADM2, there is a greater extent of VOC sensitivity, which means that addition of VOC emissions moves the chemistry in the direction of maximum  $\text{O}_3$  production efficiency, which is not the case for MOZART over much of the domain. A more extensive study would be needed to evaluate whether the conclusion that  $d[\text{O}_3]/d[\text{VOC}]$  is higher for RADM2 than for MOZART can be applied more generally. In our simulations, this effect (i.e., more  $\text{O}_3$  incremental production from VOC in RADM2 than in MOZART) appears to be dominated by other differences between the mechanisms (e.g., the inorganic rate coefficients), given that  $\text{O}_3$  concentrations predicted by MOZART are always greater than those predicted by RADM2 in our simulations. A discussion of this has been added to Section 4.3:

*“The results of the +30% VOC sensitivity studies for July indicate that  $d[O_3]/d[VOC]$  is higher (more positive) for RADM2 than for MOZART for the chemical regime represented by the models in July 2007. This shows that the two mechanisms are simulating different  $O_3$  chemical regimes – in the case of RADM2, there is greater VOC sensitivity, meaning that addition of VOC emissions moves the chemistry in the direction of maximum  $O_3$  production efficiency; this is not the case for MOZART over much of the domain. A more extensive study would be needed to evaluate whether the conclusion that  $d[O_3]/d[VOC]$  is higher for RADM2 than for MOZART can be applied more generally.”*

**9) lines 575-578: This is an interesting result which shows that differences in rate constants can account by 40% for the  $O_3$  differences between RADM2 and MOZART runs. You may highlight this result a bit more.**

This result has been highlighted further in the Abstract and in the Summary and Conclusions. In the Summary and Conclusions section, we further suggest that harmonization of inorganic rate constants could potentially lead to reduced spread in predicted  $O_3$  among multi-model studies such as AQMEII.

In the abstract, discussion of this difference now reads: *“Additionally, we found that differences in reaction rate coefficients for inorganic gas phase chemistry in MOZART- 4 vs. RADM2 accounted for a difference of  $8 \mu g m^{-3}$ , or 40% of the summertime difference in  $O_3$  predicted by the two mechanisms.”*

In the Summary and Conclusions, the text has been updated as follows. The first sentence was in the original manuscript, the second sentence has been added.

*“Although the most fundamental differences between MOZART- 4 and RADM2 (and other chemical mechanisms used in regional modeling) is the representation of VOC oxidation chemistry, we find that approximately 40% of the difference seen in predicted  $O_3$  seen in this study can be explained by differences in inorganic reaction rate coefficients employed by MOZART- 4 and RADM2. **This result suggests that harmonization of inorganic rate coefficients among chemical mechanisms used for regional air quality modeling might be valuable, and could potentially lead to a smaller spread in model-predicted  $O_3$  compared to that seen in, e.g., the multi-model studies of AQMEII (Solazzo et al., 2012b; Im et al., 2015).**”*

**10) lines 591-594: Taking into consideration all three (rate constants, deposition and photolysis schemes) it seems that altogether account about 60% for the  $O_3$  differences between RADM2 and MOZART runs. Is this correct? You may highlight this conclusion.**

It is true that if one looks at the average change in  $O_3$  concentration in these three sensitivity simulations, then a total of 60% of the MOZART-RADM2 difference in  $O_3$  concentration is explained, assuming that the effects are additive. However, the authors have consciously avoided presenting this as a conclusion in the text; since the effects of inorganic rate constants, photolysis and deposition are highly interconnected, it is reasonable to assume their combined effects may not be simply additive. We consider a quantification of the nonlinearity of this behavior to be outside the scope of this study.

**11) Figure 3: I guess here the authors refer to wind direction. Please also provide information on the approach calculating the wind direction difference between obs and model.**

The caption for Figure 3 has been fixed and now correctly refers to wind direction rather than wind speed. A more detailed description of how modeled wind direction was compared to observed wind direction has been added to Section 3.3, and reads as follows.

*“When applying these statistics to wind direction, wind direction was treated as a scalar quantity, when in fact it is a vector. This simple approach was favored rather than applying a correction (as done by, e.g., Zhang et al. (2013a) in cases where the difference in modeled vs. observed wind direction were greater than 180°). This is not expected to make an important impact on our analysis, especially since northerly winds (i.e., centered around 0°, or equivalently 360°) are not prevalent in Europe (see Figure 3 and Figure S2 in the Supplementary Material).”*

**12) Figure 16: Maybe it would be better to show the sensitivity result in a percentage scale (from -10 to 10 %).**

In Figure 16, the plot has been adjusted to show the percent difference rather than the fractional difference.

**Minor comments line 209: delete double "and". line 239: It is "for" instead of "fo". line 305: Maybe "related" instead of "associated" . line 406: It is "configuration" instead of " configuruatiun" .**

All of the above minor comments have been addressed with corrections in the text.

**lines 427-429: The sentence needs rephrasing. It is not clear.**

The sentence now reads *"Coates et al. (2016) have shown that adding representation of stagnant conditions (which were not represented in Knoté et al. (2015)) to a box model increased the sensitivity of predicted O<sub>3</sub> to the chemical mechanism, and also improved model agreement with observations."*

We believe this has improved the clarity of the original sentence, which read *"Coates et al. (2016) have shown that accounting for stagnant conditions in a box model increased the variability in predicted O<sub>3</sub> with temperature in a way that better reproduced the variability seen in observational datasets and 3-D model simulations; adding representation of stagnant conditions (which were not represented in Knoté et al. (2015)) to the box model also increased the sensitivity of predicted O<sub>3</sub> to the chemical mechanism."*

# Ozone air quality simulations with WRF-Chem (v3.5.1) over Europe: Model evaluation and chemical mechanism comparison

Kathleen A. Mar<sup>1</sup>, Narendra Ojha<sup>2</sup>, Andrea Pozzer<sup>2</sup>, and Tim M. Butler<sup>1</sup>

<sup>1</sup>Institute for Advanced Sustainability Studies, Potsdam, Germany

<sup>2</sup>Atmospheric Chemistry Department, Max Planck Institute for Chemistry, Mainz, Germany

*Correspondence to:* K. A. Mar (Kathleen.Mar@iass-potsdam.de)

1 **Abstract.** We present an evaluation of the online regional model WRF-Chem over Europe with a fo-  
2 cus on ground-level ozone (O<sub>3</sub>) and nitrogen oxides (NO<sub>x</sub>). The model performance is evaluated for  
3 two chemical mechanisms, MOZART- 4 and RADM2, for year-long simulations. Model-predicted  
4 surface meteorological variables (e.g., temperature, wind speed and direction) compared well overall  
5 with surface-based observations, consistent with other WRF studies. WRF-Chem simulations em-  
6 ploying MOZART- 4 as well as RADM2 chemistry were found to reproduce the observed spatial  
7 variability in surface ozone over Europe. However, the absolute O<sub>3</sub> concentrations predicted by the  
8 two chemical mechanisms were found to be quite different, with MOZART- 4 predicting O<sub>3</sub> concen-  
9 trations up to 20 µg m<sup>-3</sup> greater than RADM2 in summer. Compared to observations, MOZART- 4  
10 chemistry overpredicted O<sub>3</sub> concentrations for most of Europe in the summer and fall, with a sum-  
11 mertime domain-wide mean bias of +10 µg m<sup>-3</sup> against observations from the AirBase network. In  
12 contrast, RADM2 chemistry generally led to an underestimation of O<sub>3</sub> over the European domain in  
13 all seasons. We found that the use of the MOZART- 4 mechanism, evaluated here for the first time  
14 for a European domain, led to lower absolute biases than RADM2 when compared to ground-based  
15 observations. The two mechanisms show relatively similar behavior for NO<sub>x</sub>, with both MOZART- 4  
16 and RADM2 resulting in a slight underestimation of NO<sub>x</sub> compared to surface observations. Further  
17 investigation into the differences between the two mechanisms revealed that the net midday photo-  
18 chemical production rate of O<sub>3</sub> in summer is higher for MOZART- 4 than for RADM2 for most  
19 of the domain. The largest differences in O<sub>3</sub> production can be seen over Germany, where net O<sub>3</sub>  
20 production in MOZART- 4 is seen to be higher than in RADM2 by 1.8 ppb hr<sup>-1</sup> (3.6 µg m<sup>-3</sup> hr<sup>-1</sup>)  
21 or more. We also show that, while the two mechanisms exhibit similar NO<sub>x</sub>-sensitivity, RADM2 is  
22 approximately twice as sensitive to increases in anthropogenic VOC emissions as MOZART- 4. Ad-

23 ditionally, we found that differences in reaction rate coefficients for inorganic gas phase chemistry  
24 in MOZART- 4 vs. RADM2 accounted for a difference of  $8 \mu\text{g m}^{-3}$ , or 40% of the summertime dif-  
25 ference in  $\text{O}_3$  predicted by the two mechanisms. Differences in deposition and photolysis schemes  
26 explained smaller differences in  $\text{O}_3$ . Our results highlight the strong dependence of modeled surface  
27  $\text{O}_3$  over Europe on the choice of gas phase chemical mechanism, which we discuss in the context  
28 of overall uncertainties in prediction of ground-level  $\text{O}_3$  and its associated health impacts (via the  
29 health-related metrics MDA8 and SOMO35).

## 30 1 Introduction

31 Tropospheric ozone ( $O_3$ ) is an air pollutant with adverse effects on human and ecosystem health  
32 as well as a short-lived climate forcer with a significant warming effect (e.g., Monks et al., 2015;  
33 Stevenson et al., 2013; WHO, 2003). In Europe, ozone pollution remains a problem: the European  
34 Environmental Agency reports that between 2010 and 2012, 98% of Europe's urban population was  
35 exposed to  $O_3$  levels in exceedance of the WHO air quality guideline (EEA, 2014), leading to more  
36 than 6000 premature deaths annually (Lelieveld et al., 2015). This is despite the fact that European  
37 emissions of ozone precursors, in particular nitrogen oxides ( $NO_x$ ) and volatile organic compounds  
38 (VOCs), have decreased significantly since 1990. The persistence of unhealthy levels of ozone in  
39 Europe can be attributed to increases in hemispheric background ozone (Wilson et al., 2012) as well  
40 as the non-linear relationship between  $O_3$  and levels of precursor species  $NO_x$  and VOC (EEA,  
41 2014).

42 Air quality models are employed to understand the drivers of air pollution at a regional scale and to  
43 evaluate the roles of and interactions between emissions, meteorology and chemistry. These models  
44 fall into two broad categories: offline Chemistry-Transport Models (CTMs), in which meteorology is  
45 calculated separately from model chemistry, and "online" models, the category to which WRF-Chem  
46 belongs, in which the meteorology and chemistry are coupled, meaning they are solved together in  
47 a physically consistent manner (e.g., Zhang, 2008). The meteorology and chemistry components in  
48 WRF-Chem use the same horizontal and vertical grids and same timestep, eliminating the need for  
49 temporal interpolation (e.g., Grell et al., 2004, 2005).

50 Air quality modeling studies over the European region have predominantly utilized CTMs, ex-  
51 amples of which include EMEP (Simpson et al., 2012), CHIMERE (Terrenoire et al., 2015), and  
52 LOTOS-EUROS (Schaap et al., 2008). **The application of online coupled regional meteorology-**  
53 **chemistry models in Europe, among them WRF-Chem, has been recently reviewed by Baklanov**  
54 **et al. (2014). The use of WRF-Chem over Europe has increased in recent years (e.g., Forkel et al.,**  
55 **2012; Žabkar et al., 2015; Solazzo et al., 2012a, b; Tuccella et al., 2012; Zhang et al., 2013a, b). How-**  
56 **ever, only a limited number of these studies are dedicated to the evaluation of WRF-Chem-simulated**  
57 **meteorology and chemistry over the whole European domain.** The study of Tuccella et al. (2012)  
58 evaluated the performance of WRF-Chem using the RADM2 chemical mechanism by comparing  
59 domain-wide average values against observations of meteorology and chemistry. However, an eval-  
60 uation of the spatial distribution of model-simulated meteorology and trace gases is missing. This  
61 type of spatial information is extremely pertinent for air quality management applications, where  
62 model performance at a national scale can become more relevant than performance metrics applied  
63 to the whole of Europe; this information gets lost when only comparing quantities that have been  
64 averaged over the entire domain. Additionally, Tuccella et al. (2012) utilized time-invariant chem-  
65 ical boundary conditions, which the authors suggested misrepresented the seasonal changes in the  
66 intercontinental transport (Tuccella et al., 2012). **The importance of temporally varying chemical**



67 boundary conditions in air quality modeling has also been stressed in other studies (including Akri-  
68 tidis et al., 2013; Andersson et al., 2015). In addition to the study of Tuccella et al. (2012), Zhang  
69 et al. (2013b) evaluated the performance WRF-Chem-MADRID (Zhang et al., 2010), an unofficial  
70 version of WRF-Chem coupled to the Model of Aerosol Dynamics, Reaction, Ionization, and Dis-  
71 solution (MADRID), over Europe for the month of July 2001, employing the gas-phase mechanism  
72 CB05 (Yarwood et al., 2005). This detailed study provides a valuable reference for comparison to  
73 the present work, but their simulations are only for one month, rather than the complete seasonal  
74 cycle.

75 Several groups contributed WRF-Chem simulations to the AQMEII project (phase 1 and phase 2)  
76 for the European domain (Solazzo et al., 2012b; Im et al., 2015). In AQMEII phase 1, two differ-  
77 ent WRF-Chem simulations were part of the model ensemble for Europe, but evaluation of model  
78 performance for ozone focused on evaluation of the ensemble (Solazzo et al., 2012b), rather than  
79 on individual members. In fact, in the analysis of Solazzo et al. (2012b), individual models were  
80 anonymized, meaning the performance statistics for the WRF-Chem ensemble members are not ex-  
81 plicitly presented. The evaluation of model performance with respect to ozone in AQMEII phase 2  
82 (Im et al., 2015) provides more information on the model performance of the contributing WRF-  
83 Chem ensemble members for the European domain. In AQMEII phase 2, seven different WRF-Chem  
84 runs were part of the ensemble. Of these seven simulations, four of them used the gas phase chemical  
85 mechanism RADM2 (Stockwell et al., 1990), two used the mechanism CBMZ (Zaveri and Peters,  
86 1999), and one used the mechanism RACM (Stockwell et al., 1997; Geiger et al., 2003). All WRF-  
87 Chem simulations for Europe in AQMEII phase 2 tended to underestimate ozone concentrations,  
88 with annual average normalized mean bias ranging from -1.6 to -15.8 %, depending on the ensemble  
89 member.

90 The purpose of the present study is to perform a detailed evaluation of meteorology and gas phase  
91 chemistry simulated by WRF-Chem, including the spatial and seasonal variations over a full year  
92 seasonal cycle using time-varying chemical boundary conditions. This evaluation is performed for  
93 two different gas phase chemical mechanisms within WRF-Chem, MOZART- 4 (Emmons et al.,  
94 2010) and RADM2 (Stockwell et al., 1990). As discussed above, the RADM2 mechanism has been  
95 popularly used in WRF-Chem for simulation over Europe (Tuccella et al., 2012; Im et al., 2015). The  
96 MOZART- 4 chemical mechanism has been widely used with WRF-Chem for regional air quality  
97 applications outside of Europe (e.g., Pfister et al., 2013; Im et al., 2015). To the authors' knowledge,  
98 however, WRF-Chem with MOZART- 4 has not yet been applied and evaluated over a European  
99 domain.

100 The simultaneous evaluation of WRF-Chem with two different chemical mechanisms further al-  
101 lows us to evaluate the sensitivity of O<sub>3</sub> and NO<sub>x</sub> to the choice of chemical mechanism in a setup  
102 where the differences in model physics and other parameters are minimized. This is in contrast to  
103 the study of Im et al. (2015), where the various WRF-Chem ensemble members also used different

104 schemes for model physics. Coates and Butler (2015) recently investigated the sensitivity of the pro-  
105 duction of odd oxygen ( $O_x$ , a proxy for production of  $O_3$ ) to the choice of chemical mechanism using  
106 a box model, and found that choice of chemical mechanism led to differences in  $O_3$  concentrations  
107 on the order of 10 ppb under idealized conditions, although differences between the MOZART- 4  
108 and RADM2 chemical mechanisms tended to be closer to 5 ppb. In another box model study, Knote  
109 et al. (2015) investigated the sensitivity of  $O_3$ ,  $NO_x$ , and other radicals to the different gas-phase  
110 chemical mechanisms used in the models that contributed to the AQMEII phase-2 intercomparison  
111 project. Knote et al. (2015) found that the choice of chemical mechanism is responsible for a 5%  
112 uncertainty in predicted  $O_3$  concentrations and a 25% uncertainty in predicted  $NO_x$  concentrations.

113 The present study builds on the work of Coates and Butler (2015) and Knote et al. (2015) by  
114 comparing two chemical mechanisms within an online coupled regional air quality model. The use  
115 of WRF-Chem provides an advantage in that it is compatible with multiple different chemical mech-  
116 anisms, allowing us to test the effect of different chemistry with minimal confounding factors due to  
117 differences in model physics, etc. Furthermore, the use of an online regional model rather than a box  
118 model allows us to examine the sensitivity of model-predicted concentrations to the choice of chemi-  
119 cal mechanism under more realistic conditions, in which variations in meteorology and dynamics are  
120 fully included. Parameters such as radiation are allowed to vary realistically, and different chemical  
121 regimes ( $NO_x$ - vs. VOC-limited) are present (e.g., in different seasons and in different parts of the  
122 model domain).

123 Chemical mechanism comparisons have also been undertaken previously using 3-D regional air  
124 quality models, though the majority have focused on comparing the SAPRC-99 mechanism (Carter,  
125 1990) with versions of the Carbon Bond mechanism (Gery et al., 1989) over a U.S. domain (Luecken  
126 et al., 2008; Faraji et al., 2008; Yarwood et al., 2003; Zhang et al., 2012). Two additional studies have  
127 compared versions of the RACM mechanism with RADM2 (Mallet and Sportisse, 2006) and CB05  
128 (Kim et al., 2010) using the model Polyphemus (Mallet et al., 2007) for a European domain. Typ-  
129 ically, these studies found that simulations using two different chemical mechanisms led to differ-  
130 ences in  $O_3$  on the order of 5-10 ppb (Luecken et al., 2008; Zhang et al., 2012; Mallet and Sportisse,  
131 2006; Kim et al., 2010), although extreme differences of 30-40 ppb were observed between SAPRC-  
132 99 and CB-IV mechanisms when simulating high ozone episodes (Faraji et al., 2008; Yarwood et al.,  
133 2003).

134 In this paper, the model configuration, including emissions and initial and boundary conditions, is  
135 described in Section 2. A description of observational datasets for meteorology and chemistry and  
136 the evaluation methodology is provided in Section 3. Results for the model evaluation and intercom-  
137 parison of two chemical are presented in Section 4 followed by a summary and concluding remarks  
138 in Section 5.

## 139 2 Model Description and Setup

### 140 2.1 WRF-Chem

141 This study utilizes the Weather Research and Forecasting with Chemistry (WRF-Chem) model  
142 (<http://ruc.noaa.gov/wrf/WG11>) version 3.5.1. WRF-Chem has been developed collaboratively by  
143 NOAA, DOE/PNNL, NCAR and other research institutes (<https://www2.acd.ucar.edu/wrf-chem>).

144 We defined our simulation domain on the Lambert projection. The model domain is centered at  
145 15° E, 52° N, and covers nearly the entire European region. The horizontal resolution is chosen to  
146 be 45 km × 45 km. The model domain has 115 and 100 grid points in the west-east and south-north  
147 directions respectively.

148 We have used 35 vertical levels in the model starting from surface to 10 hPa. The lowest model  
149 level corresponds to an approximate altitude of 50 m above the surface. Tests have shown that surface  
150 layer concentrations in this configuration are effectively the same as when the lowest model level  
151 is at a height of 14 m, but with no urban surface physics scheme (the urban physics scheme is  
152 incompatible with a 14-m model level). Geographical data including terrain height, soil properties,  
153 albedo, etc. are interpolated primarily from USGS (United States Geological Survey data (Wang  
154 et al., 2014)) at 30 sec resolution. The land use classification has been interpolated from the CORINE  
155 data (EEA, 2012) at 250 m resolution, which was then mapped to the USGS land use classes used  
156 by WRF (see Kuik et al., 2016).

157 Model simulations are conducted for the period of 23 December 2006 to 31 December 2007.  
158 The first week of output was treated as model spin up and has been discarded. The instantaneous  
159 model output, stored every hour, has been used for the analysis. The different options used in this  
160 study to parametrize the atmospheric processes are listed in Table 1. A namelist is available in the  
161 Supplementary Material.

162 The initial and lateral boundary conditions for the meteorological fields were provided from the  
163 ERA-interim reanalysis dataset available from ECMWF (<http://www.ecmwf.int/en/research/climate-reanalysis/era-interim>). This data is available every 6 hours with a spatial resolution of approximately 80 km  
164 (T255 spectral). In order to limit the errors in the WRF simulated meteorology the Four Dimensional  
165 Data Assimilation (FDDA) has been applied. In the FDDA, temperature is nudged at all the vertical  
166 levels with a nudging coefficient of 0.0003. The horizontal winds are nudged at all the vertical levels,  
167 except within the PBL, with the nudging coefficient of 0.0003. Sensitivity studies performed showed  
168 that nudging of water vapor highly suppressed the precipitation over Europe in a manner inconsis-  
169 tent with observations. As such, water vapor is not nudged in our simulations. This also follows the  
170 approach of, e.g., Miguez-Macho et al. (2004) and Stegehuis et al. (2014). The nudging coefficients  
171 for temperature and winds have been chosen following previous studies (Stauffer et al., 1991; Liu  
172 et al., 2012). The time step for the simulations has been set at 180 s.

174 Initial and boundary conditions for chemical fields in WRF-Chem are used from the MOZART-  
175 4/GEOS5 simulations (<http://www.acd.ucar.edu/wrf-chem/mozart.shtml>), with a horizontal resolu-  
176 tion of  $1.9^\circ \times 2.5^\circ$  and 56 pressure levels. MOZART- 4/GEOS-5 simulations use meteorology from  
177 the NASA GMAO GEOS-5 model and emissions based on ARCTAS inventory ([http://www.cgrer.  
178 uiowa.edu/arctas/emission.html](http://www.cgrer.uiowa.edu/arctas/emission.html)).

## 179 **2.2 Emissions**

180 Anthropogenic emissions of CO, NO<sub>x</sub>, SO<sub>2</sub>, NMVOCs, PM<sub>10</sub>, PM<sub>25</sub>, and NH<sub>3</sub> are used from the  
181 TNO-MACC II emission inventory for Europe (Kuenen et al., 2014), for the year 2007. These emis-  
182 sions are provided as yearly totals by source sector on a high-resolution (7 km × 7 km) grid. The  
183 TNO-MACC II emission inventory is based on emissions reported by member countries to the Eu-  
184 ropean Monitoring and Evaluation Program (EMEP), which are then further refined to fill gaps and  
185 correct errors and obvious inconsistencies. Emissions are temporally disaggregated based on sea-  
186 sonal, weekly and diurnal cycles provided by Denier van der Gon et al. (2011); Schaap et al. (2005).  
187 These temporal profiles vary by source sector according to the SNAP (Selected Nomenclature for  
188 Sources of Air Pollution) convention. NMVOC emissions are split into modeled NMVOC species  
189 (e.g., ethane, aldehydes) based on von Schneidmesser et al. (2016). NO<sub>x</sub> is emitted as 90% NO and  
190 10% NO<sub>2</sub> by mole. Emissions are distributed into the first seven model vertical layers (the surface  
191 and the first 6 model layers above the surface) based on sectoral averages from (Bieser et al., 2011),  
192 although model runs showed little sensitivity to the distribution of emissions above the surface layer.

193 The model domain used in this study is larger than the European domain used in the TNO-  
194 MACC II inventory (Kuenen et al., 2014). Emissions at our domain edges were filled using the  
195 Hemispheric Transport of Air Pollution (HTAP v2.2) emission inventory for the year 2008 ([http://  
196 edgar.jrc.ec.europa.eu/htap\\_v2/index.php](http://edgar.jrc.ec.europa.eu/htap_v2/index.php)). The HTAP v2 data, described in detail by Janssens-  
197 Maenhout et al. (2015), is harmonized at a spatial resolution of  $0.1^\circ \times 0.1^\circ$  and available with  
198 monthly time resolution. In our model simulations, no additional weekly or diurnal profiles were  
199 applied to the HTAP v2 emissions. Furthermore, all emissions from HTAP were emitted into the  
200 surface model layer. Because HTAP emissions were only used at the grid "edge," the differences in  
201 temporal and vertical resolution of emissions used for HTAP is not expected to have a significant  
202 impact on model results. An example of emissions processed for model input is shown Figure S1 in  
203 the Supplementary Material.

204 Biomass burning emissions are from the Fire Inventory from NCAR (FINN), Version 1 (Wiedin-  
205 myer et al., 2011). To avoid the double counting of emissions from agricultural burning (i.e., assum-  
206 ing that the FINN product captures large-scale agricultural burning), emissions of the combustion  
207 species CO, NO<sub>x</sub>, and SO<sub>2</sub> from SNAP category 10 (Agriculture) in the TNO-MACC II inventory  
208 were not included in model simulations, at the suggestion of H.A.C. van der Gon (personal commu-

209 nication, 2015). Biogenic Emissions are calculated online based on weather and land use data using  
210 the Model of Emissions of Gases and Aerosols from Nature (MEGAN) (Guenther et al., 2006).

### 211 **2.3 Model Chemistry**

212 The two year-long WRF-Chem simulations performed for this study are summarized in Table 2. In  
213 the MOZART simulation, gas phase chemistry is represented by the Model for Ozone and Related  
214 chemical Tracers, version 4 (MOZART- 4) mechanism (Emmons et al., 2010). Tropospheric chem-  
215 istry is represented by 81 chemical species, which participate in 38 photolysis and 159 gas-phase  
216 reactions. The MOZART- 4 mechanism includes explicit representation of the NMVOCs ethane,  
217 propane, ethene, propene, methanol, isoprene, and  $\alpha$ -pinene. Other NMVOC species are represented  
218 by lumped species based on the reactive functional groups. In the WRFV3.5.1 code, two bug fixes  
219 have been included for the MOZART- 4 mechanism: the  $\text{NH}_3+\text{OH}$  rate coefficient has been cor-  
220 rected following Knote et al. (2015), and a correction has been made to treatment of the vertical  
221 mixing of MOZART- 4 species (A.K. Peterson, personal communication). In the WRF-Chem sim-  
222 ulations, we use the version of MOZART- 4 coupled to the simple GOCART aerosols mechanism  
223 (Ackermann et al., 1998b), known as the MOZCART mechanism. In this paper, we limit our anal-  
224 ysis to gas-phase species. Because of this focus, and to simplify the interpretation the mechanism  
225 intercomparison (see below), all aerosol radiative feedbacks (i.e., both direct and indirect effects) are  
226 turned off in all model simulations in this study.

227 In the RADM2 simulation, gas phase chemistry is represented by the second generation Regional  
228 Acid deposition Model (RADM2) (Stockwell et al., 1990). This mechanism has 63 chemical species  
229 which participate in 21 photolysis and 136 gas phase reactions. The NMVOC oxidation in RADM2 is  
230 treated in a less-explicit fashion than in MOZART, in which ethane, ethene and isoprene are the only  
231 species treated explicitly and all other NMVOCs are assigned to lumped species based on OH reac-  
232 tivity and molecular weight. In WRF-Chem, RADM2 is coupled to the MADE/SORGAM aerosol  
233 module, which is based on the Modal Aerosol Dynamics Model for Europe (MADE) (Binkowski  
234 and Shankar, 1995; Ackermann et al., 1998a) and Secondary Organic Aerosol Model (SORGAM)  
235 (Schell et al., 2001). However, as noted above, in this study we focus our analysis on gas-phase  
236 chemistry.

237 In both the RADM2 and MOZART simulations, the chemical mechanism code was generated  
238 with the Kinetic Pre-Processor (KPP) (Damian et al., 2002; Sandu and Sander, 2006), and equations  
239 are solved using a Rosenbrock-type solver. Note that when using RADM2 chemistry, there are two  
240 different solvers available within WRF-Chem. We chose to use the KPP chemistry and Rosenbrock  
241 solver to be consistent with the MOZART runs, and also because the alternative QSSA chemistry  
242 solver has been shown to have problems representing  $\text{NO}_x$  titration (Forkel et al., 2015). In partic-  
243 ular, the QSSA treatment of RADM2 chemistry was found to result in an under-representation of  
244 nocturnal ozone titration for areas with high  $\text{NO}$  emissions.

## 245 **3 Observational datasets**

246 A summary of the observational datasets used for model evaluation can be found in Table 3.

### 247 **3.1 Meteorology**

248 Since WRF-Chem couples the meteorology simulations online with the chemistry, we begin by eval-  
249 uating the modeled meteorological fields against observations which are driving the simulations of  
250 chemical fields. In this study, the WRF-Chem simulated meteorological fields are evaluated against  
251 the in situ measurements of mean sea level pressure (MSLP), 2-meter temperature (T2) and 10-meter  
252 wind speed and direction (WS10 and WD10, respectively) from the Global Weather Observation  
253 dataset provided by the British Atmospheric Data Center (BADC). We chose these meteorologi-  
254 cal variables for the evaluation as these are expected to have the most significant influence on the  
255 gas-phase chemistry, which is the main focus of this study.

### 256 **3.2 Chemistry**

#### 257 **3.2.1 EMEP Network**

258 The EMEP observational dataset provides surface measurements of pollutant concentrations, in-  
259 cluding tropospheric ozone and its precursors, at stations chosen to be representative of regional  
260 background pollution (see, e.g., Tørseth et al., 2012). The regional focus is in keeping with the goals  
261 of the Convention on Long-range Transboundary Air Pollution (CLRTAP), under which this network  
262 is administrated.

#### 263 **3.2.2 AirBase Network**

264 AirBase is the public air quality database of the European Environmental Agency (EEA), and repre-  
265 sents a much denser network of monitoring than the EMEP network ([http://www.eea.europa.eu/data-  
266 and-maps/data/airbase-the-european-air-quality-database-7](http://www.eea.europa.eu/data-and-maps/data/airbase-the-european-air-quality-database-7)). Because of the relatively coarse hori-  
267 zontal resolution in this model study, model output is only compared against AirBase stations that  
268 are classified as "rural background." **The station classification was taken from the metadata provided  
269 by the EEA for AirBase.** Some AirBase stations are also part of the EMEP network; the subset  
270 of AirBase stations used in this study exclude any stations that are also part of the EMEP network  
271 (since they are already included in the evaluation against EMEP observations).

### 272 **3.3 Evaluation methodology**

273 Stations were excluded from our season-by-season analysis if the temporal coverage was less than  
274 75%, i.e., if missing or flagged hourly (or 3-hourly) data represented more than 25% of the hourly  
275 (or 3-hourly) time series over the entire season. For sensitivity studies that consider the month of

276 July only, stations were considered that had at least 75% temporal coverage for the month. This  
277 criteria was applied for all meteorological and chemistry observations. For comparison of model  
278 output to in situ observations, the model gridcell that is closest to the latitude, longitude location  
279 of the measurement station was chosen. Statistics calculated include the mean, mean bias (MB),  
280 normalized mean bias (NMB), mean fractional bias (MFB) and the temporal correlation coefficient  
281 ( $r$ ). The domain-wide statistics presented in Tables 4 - 9 were calculating by first calculating the  
282 statistical quantity hour-by-hour at each station, and then averaging these values over all times (in  
283 the season) and all stations. Definitions of calculated statistical quantities can be found in Appendix  
284 B.

285 When applying these statistics to wind direction, wind direction was treated as a scalar quantity,  
286 when in fact it is a vector. This simple approach was favored rather than applying a correction (as  
287 done by, e.g., Zhang et al. (2013a) in cases where the difference in modeled vs. observed wind  
288 direction were greater than  $180^\circ$ ). This is not expected to make an important impact on our analysis,  
289 especially since northerly winds (i.e., centered around  $0^\circ$ , or equivalently  $360^\circ$ ) are not prevalent in  
290 Europe (see Figure 3 and Figure S2 in the Supplementary Material).

291 From hourly concentrations of  $O_3$ , both observed and modeled, additional ozone metrics for  
292 health impacts are calculated. MDA8 is defined as the maximum daily 8-hour mean ozone, in ac-  
293 cordance with the European Union's Air Quality Directive. Note that, for calculation of MDA8,  
294 a missing value was assigned if one or more hours of data in the 8-hour average were missing.  
295 SOMO35 is an indicator of cumulative annual ozone exposure used in health impact assessments.  
296 The accumulated health impact is assumed to be proportional to the sum of concentrations above a  
297 cutoff of 35 ppb, chosen because the relationship between  $O_3$  and adverse effects is very uncertain  
298 below this threshold (WHO, 2013). Mathematically, SOMO35 is defined as the sum of MDA8  
299 levels over 35 ppb ( $70 \mu\text{g m}^{-3}$ ) over a year, in units of concentration-days, following Amann et al.  
300 (2008).

$$301 \text{ SOMO35} = \frac{365}{N_{\text{valid}}} \sum_{\text{iday}} \max(0, C_{\text{iday}} - 70 \mu\text{g m}^{-3})$$

302 where  $N_{\text{valid}}$  is the number of valid (i.e., non-missing) daily values.

## 303 4 Results and Discussion

### 304 4.1 Evaluation of Meteorology

305 Table 4 shows a summary of domain-wide statistics evaluating the MOZART model simulation  
306 against observations of meteorological variables MSLP, T2, WS10 and WD10; the spatial distri-  
307 bution of these statistics shown in Figures 1-3 for temperature and wind variables. Differences in  
308 predicted meteorology between the MOZART and RADM2 simulations are small, with differences  
309 in MSLP less than one hundredth of 1%, and differences in T2, WS10, and WD10 generally far

310 below 1%. Since the simulations were run without aerosol-radiative feedbacks, it was expected that  
311 the two simulations would show minimal differences in meteorology, and we conclude that differ-  
312 ences in O<sub>3</sub> and NO<sub>x</sub> predicted in the MOZART and RADM2 simulations (Section 4.2) are a direct  
313 result of differences in the chemistry, rather than chemistry-radiative feedbacks. Statistics for me-  
314 teorology for the RADM2 simulation can be found in the Supplementary Material, Table S1 and  
315 Figures S4-S7.

316 MSLP has been reproduced over the entire European domain with a high degree of skill in every  
317 season for both simulations, with negligible bias (domain-averaged NMB and MFB are zero in all  
318 seasons) and temporal correlation coefficients (r values) of 0.98 or greater (see also Figures S3 and  
319 S7 in the Supplementary Material).

320 The spatial distribution of seasonal average T2 in the model and observations is shown in Figure 1,  
321 along with the spatial variation in mean bias and temporal (3-hourly) correlation. Overall, the spatial  
322 variability in measured T2 is found to be well-reproduced by WRF-Chem during all the seasons. The  
323 absolute values of mean biases in T2 were generally found to be lower than 1° C. Larger biases in T2  
324 can be found in the Alps, in particular during winter, where T2 is often overpredicted by more than  
325 1° C (Figure 1). This larger bias over mountainous regions, also found in a previous study (Zhang  
326 et al., 2013a), is likely due to the complex mountain terrain and related unresolved local dynamics.  
327 The r values are generally found to be more than 0.9 in all the seasons and show no significant  
328 geographical variation, indicating that the model is able to reproduce the hourly variations in near  
329 surface temperature. Averaged over the entire domain, the mean bias in T2 varies from -0.4 to +  
330 0.3° C depending on the season (Table 4).

331 The spatial variability in wind speeds, including the seasonality, with strongest winds during the  
332 winter, have been reproduced by the model (Figure 2). However, the model tends to overestimate  
333 winds speeds with larger biases (2 m/s or more) during the winter and fall. The regions showing  
334 greater bias in wind speed include the Alps, coastal regions, and the low-lying areas of northern  
335 Germany and Denmark (Figure 2). The temporal correlation of wind speed is generally above 0.7 in  
336 the northern half of the domain, but is lower (0.4-0.6) in the southern part of the domain, in areas  
337 in the Alps and close to the Mediterranean (Figure 2). Similar behavior for modeled wind speed is  
338 reported by Zhang et al. (2013a), who attributes the overestimation in wind speeds primarily to poor  
339 representation of surface drag exerted by unresolved topographical features, which results in model  
340 limitations in simulating circulation systems such as sea breeze and bay breeze. An overview of the  
341 statistics for wind direction is presented in Table 4, with the spatial distribution shown in Figure 3.  
342 Wind direction over the continent is predominantly from the west and south, and the mean bias in  
343 wind direction is between 20 and 30 degrees depending on the season. Similar to the patterns seen  
344 for wind speed, areas with complex topography (the Alps, the Balkans, the Mediterranean coast)  
345 show the largest biases and the lowest correlations for wind direction.



346 Overall, we find that WRF-Chem is capable of reproducing the spatial and temporal variations  
347 in the European meteorological conditions reasonably well, in a manner consistent with previous  
348 studies (e.g. Zhang et al., 2013a).

## 349 4.2 Evaluation of Chemistry

### 350 4.2.1 Ozone

351 We begin the evaluation of chemistry by examining the seasonal average surface  $O_3$  distribution  
352 over Europe from the MOZART simulation, as shown in Figure 4. Predicted surface  $O_3$  distributions  
353 show a clear seasonality, with maximum concentrations during summer. In all seasons, surface  $O_3$   
354 concentrations are highest over the Mediterranean region, with values during the spring and summer  
355 greater than  $110 \mu\text{g m}^{-3}$ . Simulated concentrations reproduce the north-south gradient in  $O_3$  seen  
356 in the ground-based observations. Figure 5 provides another comparison of seasonal average  $O_3$   
357 distributions in the model vs. the observations (from both the AirBase and EMEP networks) and  
358 additionally shows the spatial distribution of MB and r, the temporal (hourly) correlation coefficient;  
359 performance statistics are shown in Table 5 (against observations from the AirBase network) and  
360 Table 6 (against observations from the EMEP network). MOZART overpredicts  $O_3$  concentrations  
361 for most of Europe in the summer and fall. In winter and spring, MOZART tends to underestimate  $O_3$   
362 in north-central Europe, but overestimate  $O_3$  in southern Europe. Hourly correlation coefficients for  
363  $O_3$  are highest (greater than 0.6) in northern Europe (especially France, Germany, and the Benelux  
364 region) and in Spain, but are lower (with values of approximately 0.4) throughout Italy and the  
365 mountainous regions of the Alps. Notably, Italy and the Alps are the regions within our domain  
366 that exhibit the highest biases and lowest correlations with respect to wind direction and speed  
367 (Section 4.1), which could explain the poorer temporal correlation for  $O_3$  in these areas.

368 Looking at Tables 5 and 6, we see some differences in the statistical performance of the MOZART  
369 simulation when compared to the EMEP vs. the AirBase observational datasets. Considering the  
370 EMEP observations over the whole domain (Table 6), MOZART slightly overpredicts  $O_3$  in sum-  
371 mer, with a summertime mean bias of  $4 \mu\text{g m}^{-3}$ , whereas the summertime mean bias when compared  
372 the AirBase network is  $10 \mu\text{g m}^{-3}$  (Table 5). In winter and spring, the bias (MB, NMB, and MFB)  
373 in MOZART-predicted  $O_3$  is more negative when compared to EMEP observations than to AirBase  
374 observations. In fall, the sign of the domain-average bias changes if considering the model perfor-  
375 mance against EMEP vs. AirBase observations. These differences likely reflect differences in the  
376 character of the two observational networks. First, we expect that the Airbase rural background sites  
377 considered here may be, on average, more influenced by local pollution sources than the EMEP  
378 sites, which are selected to be representative of more remote regional background. Secondly, the ge-  
379 ographical coverage of AirBase vs. EMEP sites for  $O_3$  is slightly different (Figure S8). In particular,  
380 coverage of the U.K. and the Nordic countries is almost exclusively via the EMEP network, poten-

381 tially giving the EMEP observations a northern bias in comparison to the AirBase-only sites. Both  
382 features of the measurement networks could explain the lower values of the domain-wide average  
383  $O_3$  observed at the EMEP vs. the AirBase stations.

384 In addition to evaluating the model's ability to simulate hourly  $O_3$  concentrations, we also con-  
385 sider MDA8 and SOMO35, two metrics designed to evaluate the impact of ozone on health. The  
386 distribution of seasonal average values of MDA8 is shown in Figure 6 for the MOZART simulation.  
387 The European Union's Air Quality Directive states that, as a long-term objective, MDA8 should not  
388 exceed the threshold value of  $120 \mu\text{g m}^{-3}$ ; as a target value this long-term objective should not be  
389 exceeded on more than 25 days per year, averaged over 3 years. Figure 6 shows that, at some stations  
390 in the Alps and in southern Italy during summer, the average value of MDA8 exceeds  $120 \mu\text{g m}^{-3}$ .  
391 As seen in Figure 7, the number of days when MDA8 exceeds the  $120 \mu\text{g m}^{-3}$  is greater than 25 in  
392 spring alone for much of southern Europe, which is also captured well by the MOZART simulation.  
393 MOZART tends to overpredict MDA8 and the days in exceedance of the target value in summer and  
394 fall, consistent with the overestimation of hourly average  $O_3$  during this season. Since the metric  
395 MDA8 is, in effect, a measure of daytime ozone, it is always higher than the straight average of  
396 hourly concentrations. As a consequence, MOZART shows greater bias in MDA8 than in average  
397  $O_3$  in seasons where average  $O_3$  is already overpredicted (Tables 5 and 6). In general, regional and  
398 seasonal patterns for MDA8 simulated by MOZART are similar to those for simulated average  $O_3$ .  
399 SOMO35, an indicator for cumulative annual exposure, is shown in Figure 8 for the year 2007.  
400 MOZART is able to reproduce the north-south gradient of SOMO35 seen in the observations quite  
401 well, while overpredicting the magnitude of SOMO35 by  $2 \text{ mg m}^{-3} \cdot \text{days}$  (Table 7).

402 WRF-Chem simulations using the RADM2 chemical mechanism show a spatial and seasonal  
403 distribution of surface  $O_3$  over Europe (Figures 9 and 10) that is qualitatively similar to that for  
404 MOZART. The correlation coefficients for the MOZART and RADM2 simulations are also similar  
405 in both magnitude in distribution (Figures 5 and 10. **Absolute  $O_3$  concentrations are most similar**  
406 **(i.e., less than 5% different) between the mechanisms near the northwest edges of the domain (see**  
407 **Figures 4 and 9), where the prevailing westerly winds (Supplementary Material, Figure S2) mean**  
408 **that  $O_3$  imported from the boundary conditions plays a dominant role.** However, it is striking to  
409 note that the surface  $O_3$  concentrations predicted by two different chemical mechanisms are gen-  
410 erally quite different, with RADM2 predicting average surface  $O_3$  values that are approximately  
411  $20 \mu\text{g m}^{-3}$  lower than those predicted by MOZART in spring and summer (c.f. Figures 4 and 9,  
412 Tables 5 and 8, and Tables 6 and 9). In contrast to MOZART, RADM2 underpredicts  $O_3$  through-  
413 out most of Europe in all seasons. An exception to this is in southern Europe in winter, where  
414 RADM2, like MOZART, shows some overprediction of  $O_3$  concentrations in southern Europe, par-  
415 ticularly near the Mediterranean. RADM2 also overpredicts  $O_3$  near the Mediterranean in fall (a  
416 season where MOZART overpredicts  $O_3$  Europe-wide). The general underprediction of  $O_3$  con-  
417 centrations in RADM2 means that the health metrics MDA8 and SOMO35 are also underpredicted

418 (Tables 7- 8 and Figure 8). Overall, absolute biases (i.e., the absolute value of MB, NMB, and MFB)  
419 are smaller for MOZART than for RADM2, indicating that MOZART is more successful overall in  
420 reproducing European ground-level O<sub>3</sub>.

421 Model biases for O<sub>3</sub> in both the MOZART and RADM2 simulations are in line with biases found  
422 in other regional modeling studies for Europe. For instance, values for the NMB in European sum-  
423 mertime O<sub>3</sub> ranged from less than -20% to greater than +20% depending on the ensemble member  
424 in AQMEII (Solazzo et al., 2012b; Im et al., 2015), compared to values of -18% and +14% for the  
425 RADM2 and MOZART simulations, respectively, in the present study. Zhang et al. (2013b) found  
426 domain-wide values for NMB for O<sub>3</sub> ranging from +4.2% to +19.1% for the month of July 2001,  
427 depending on their model configuration. Tuccella et al. (2012) report a domain-average mean bias in  
428 O<sub>3</sub> of -1.4 μg m<sup>-3</sup> averaged over the whole year. Although the work of Tuccella et al. (2012) uses  
429 the RADM2 chemical mechanism and simulates the year 2007, similar to the RADM2 simulation in  
430 the present study, there are several differences in model configuration that could explain the observed  
431 differences in predicted O<sub>3</sub>, including the use of time-invariant chemical boundary conditions, the  
432 use of the QSSA rather than the Rosenbrock chemical solver (which has been shown to make a  
433 difference Forkel et al. (see 2015)), and the use of an alternate emissions inventory (from EMEP).

434 The temporal correlation with hourly measurements for O<sub>3</sub> in this study are also in line with  
435 other regional modeling studies of O<sub>3</sub> for Europe. Simulations with both chemical mechanisms lead  
436 to reasonable correlations between the model-predicted and observed O<sub>3</sub> concentrations over the  
437 entire domain, with r values generally in the range of 0.6-0.8 (Figures 5 and 10, Tables 5 and 8).  
438 This is consistent with the hourly correlation coefficient for O<sub>3</sub> of 0.62 reported by Tuccella et al.  
439 (2012), where their r value represents an average over the entire year of 2007. Zhang et al. (2013b)  
440 also report correlation coefficients of 0.6-0.7 for hourly O<sub>3</sub> over the European domain (horizontal  
441 resolution 0.5°) using the CB05 gas-phase chemical mechanism in WRF-Chem.

442 In addition to evaluating the performance of the MOZART and RADM2 simulations on their abil-  
443 ity to reproduce ground-level ozone concentrations, we compare the observed sensitivity of modeled  
444 O<sub>3</sub> to the choice of chemical mechanism to other studies that have investigated the uncertainty in 3-D  
445 model predictions associated with the choice of chemical mechanism. Knote et al. (2015) used box  
446 model simulations based on AQMEII phase 2, and concluded that the uncertainty in predicted O<sub>3</sub> in  
447 a 3-D model solely due to the choice of gas phase chemical mechanism should be of the order of 5%,  
448 or 4 ppbv (8 μg m<sup>-3</sup>). This is quite a bit smaller than the sensitivity to chemical mechanism found  
449 in this study, where we see differences in summertime average O<sub>3</sub> of 20 μg m<sup>-3</sup>, corresponding to a  
450 relative difference of approximately 40%. Coates et al. (2016) have shown that adding representation  
451 of stagnant conditions (which were not represented in Knote et al. (2015)) to a box model increased  
452 the sensitivity of predicted O<sub>3</sub> to the chemical mechanism, and also improved model agreement  
453 with observations. This result suggests that day-to-day variability in meteorological conditions and

454 transport can enhance the sensitivity of  $O_3$  to chemical mechanism compared to what is seen in box  
455 models.

456 Another interesting basis for comparison is the study of Mallet and Sportisse (2006), who investi-  
457 gate uncertainty in the CTM Polyphemus due to various physical parameterizations, including chem-  
458 ical mechanism (comparing RACM and RADM2), using an ensemble approach. They estimated an  
459 overall uncertainty in  $O_3$  concentrations of 17% based on choices for physical parameterizations in  
460 general, but identified the choice of chemical mechanism along with the turbulent closure parame-  
461 terization as the two most important drivers of this uncertainty. Simulations using the RACM vs.  
462 RADM2 mechanisms yielded differences in average  $O_3$  concentrations of 7-13  $\mu\text{g m}^{-3}$ , depending  
463 on the other parameterizations used. It is clear that the sensitivity of  $O_3$  to the use of the MOZART  
464 vs. RADM2 chemical mechanism in this study is large compared to other studies of mechanism  
465 comparisons in 3-D models (see also Luecken et al., 2008; Kim et al., 2010)), though even larger  
466 absolute differences in hourly  $O_3$  concentrations (up to 40 ppb, or 80  $\mu\text{g m}^{-3}$ ) have been found in  
467 studies of episodic ozone (Faraji et al., 2008; Yarwood et al., 2003). It is possible that MOZART  
468 and RADM2 as implemented in this study are examples of chemical mechanisms that are extremely  
469 different from one another on a spectrum of other commonly-used mechanisms; the differences be-  
470 tween the two mechanisms will be further explored in Section 4.3.

#### 471 **4.2.2 Nitrogen oxides**

472 Seasonal average surface-level  $\text{NO}_x$  for the MOZART simulation are shown in Figure 11. Several  
473 hotspots in the spatial distribution of  $\text{NO}_x$  mixing ratios are apparent, as expected based on the  
474 intensity of emissions in these areas.  $\text{NO}_x$  hotspots with concentrations of more than 30  $\mu\text{g m}^{-3}$   
475 are visible over parts of France, Belgium, Germany and Russia. Similar high concentrations are  
476 also seen over the marine regions close to Barcelona, Monaco, and southern France. As shown  
477 in Table 5, the MOZART simulation slightly underpredicts domain-average  $\text{NO}_x$  concentrations  
478 for all seasons when comparing to AirBase observations. In Figures 12 and 13 we examine the  
479 spatial distribution of  $\text{NO}_x$  broken down into its components,  $\text{NO}_2$  and  $\text{NO}$ , together with the spatial  
480 distribution of MB and r. The MOZART simulation overestimates  $\text{NO}_2$  in the U.K., northern France,  
481 Belgium, and central Germany, all of which are regions known for having high  $\text{NO}_x$  emissions and  
482 concentrations. However this does not hold true for the Netherlands, a neighboring region with high  
483 emissions where MOZART tends to underpredict rather than overpredict  $\text{NO}_2$  concentrations.  $\text{NO}$ ,  
484 on the other hand, is significantly underpredicted compared to surface measurements throughout  
485 the domain. This may be partially due to the relatively coarse horizontal resolution of the model, in  
486 which fresh  $\text{NO}$  emissions are immediately diluted over a large area, and could also be a consequence  
487 of model deficiencies in representing  $\text{NO}_x$  chemical cycles. Artifacts related to reporting of low  
488  $\text{NO}$  concentrations approaching measurement detection limits could also play a role (observed time

489 series for NO typically show a baseline of 1-2  $\mu\text{g m}^{-3}$ , whereas modeled concentrations reach a  
490 baseline of zero).

491 Domain average temporal correlation coefficients ( $r$ ) against hourly measurements of  $\text{NO}_x$ ,  $\text{NO}_2$ ,  
492 and NO (Tables 5 and 6) range from approximately 0.2 to 0.5, which is lower than correlations for  
493  $\text{O}_3$  but consistent with other studies, discussed further below. In all seasons, the domain-averaged  
494 temporal correlation coefficient is higher when compared to EMEP vs. AirBase observations. This  
495 is attributed to lesser local influences and therefore better regional representativeness of the EMEP  
496 stations. No exceptional patterns are seen in the spatial distribution of  $r$  for  $\text{NO}_2$  or NO, although  
497 correlation appears slightly better in the northern part of the domain. The MOZART simulation  
498 shows the highest domain-average correlation coefficients ( $r$ ) for  $\text{NO}_x$ ,  $\text{NO}_2$ , and NO in winter and  
499 fall, and the lowest domain-average  $r$  values in summer.

500  $\text{NO}_x$  predicted by the RADM2 simulation shows fairly similar behavior to  $\text{NO}_x$  predicted by  
501 the MOZART simulation (cf. Figures 12 and 14 and additional Figures S10-S11 in the Supple-  
502 mentary Material). In general, simulated  $\text{NO}_x$  concentrations are slightly higher for MOZART than  
503 for RADM2. Domain-wide average  $\text{NO}_x$  concentrations predicted by MOZART are approximately  
504  $2 \mu\text{g m}^{-3}$  higher than for RADM2 in all seasons except winter, where the difference is approximately  
505  $3 \mu\text{g m}^{-3}$  (cf. Tables 5 and 8). The spatial distribution of MB for  $\text{NO}_2$  for the RADM2 simulation  
506 generally shows the same patterns as observed for the MOZART simulation, namely a slight over-  
507 estimation in the U.K., northern France, Belgium, and central Germany. Like for MOZART, NO  
508 for RADM2 is underpredicted throughout the domain, with NO concentrations slightly more neg-  
509 atively biased than in MOZART in all seasons except Fall, when NO concentrations are higher for  
510 RADM2 than for MOZART and show better agreement with the observations. Temporal correlation  
511 for  $\text{NO}_2$  and NO in RADM2 is also found to show similar behavior to the MOZART simulation.  
512 An exception to the similarity observed between the mechanisms for  $\text{NO}_x$  can be seen over central  
513 Germany in winter, where MB values for  $\text{NO}_2$  are 6-10  $\mu\text{g m}^{-3}$  for MOZART (Figure 12), but in the  
514 range of 0-6  $\mu\text{g m}^{-3}$  for RADM2 (Figure 14). Differences in  $\text{NO}_x$  concentrations predicted by the  
515 MOZART vs. RADM2 simulations are generally less than 20%, consistent with Knote et al. (2015),  
516 who conclude that uncertainty due to choice in chemical mechanism leads to an uncertainty of up to  
517 25% in 3-D model simulations.

518 Performance of the present simulations with respect to  $\text{NO}_2$  can also be compared to previous  
519 published studies (note that none of the above-cited studies perform a validation for NO or  $\text{NO}_x$ ).  
520 Zhang et al. (2013b) reports NMB values of approximately -15% for  $\text{NO}_2$  for WRF-Chem simu-  
521 lations against hourly AirBase measurements for July 2001, in line with values of -12% and -19%  
522 for the MOZART and RADM2 simulations in this study, respectively. Tuccella et al. (2012) report a  
523 MB for  $\text{NO}_2$  of  $-0.9 \mu\text{g m}^{-3}$  averaged over the whole year; for comparison the RADM2 simulation  
524 in this study shows a MB in the range of  $-2.5$  to  $-1 \mu\text{g m}^{-3}$  for fall, spring and summer, but a MB of

525  $+0.67 \mu\text{g m}^{-3}$  in summer. Evaluation of  $\text{NO}_2$  was not treated in detail in the AQMEII studies, but  
526 Im et al. (2015) report that the models for the European domain underestimate  $\text{NO}_2$  by 9% to 45%.

### 527 **4.3 Characterization of MOZART vs. RADM2 differences**

528 In this section, we explore the differences in surface  $\text{O}_3$  between the MOZART and RADM2 simula-  
529 tions by examining net  $\text{O}_3$ ,  $\text{NO}_2$ , and  $\text{NO}$  production rates as well as the  $\text{NO}_x$ - and VOC-sensitivity  
530 of the two mechanisms. We further conducted sensitivity simulations to investigate the relative con-  
531 tributions of different sources to the observed differences in surface  $\text{O}_3$  predicted by MOZART and  
532 RADM2. The month of July was chosen for the sensitivity simulations since  $\text{O}_3$  concentrations over  
533 Europe are highest during summer, and thus summer is most the most important season when con-  
534 sidering air quality exceedances and health impacts of  $\text{O}_3$ . Additionally, MOZART and RADM2  
535 show the largest differences in predicted  $\text{O}_3$  during this season (see Tables 5 and 8).

536 To gain insight into model behavior for  $\text{O}_3$ , we added terms to the model output representing  
537 hourly accumulated tendencies, i.e., the change in concentration of a species due to photochemistry  
538 only, for July simulations using MOZART and RADM2. The hourly net photochemical production  
539 rate was calculated as the difference in the accumulated tendency from one timestep to another. Fig-  
540 ure 15 shows the average of the midday (11:00-14:00 CEST, or 9:00-12:00 UTC) photochemical  
541 production rate of  $\text{O}_3$  and  $\text{NO}_x$  components for both the MOZART and RADM2 simulations. (Note  
542 that the net photochemical production rate is shown here in  $\text{ppb hr}^{-1}$  for more intuitive comparison  
543 of production and loss of the different species on a mole basis;  $\mu\text{g m}^{-3}$  was used in Section 4.2 be-  
544 cause this is the unit in which limit and target values in the EU Air Quality Directive are expressed.)

545 Overall, the spatial variability as well as the magnitudes of net  $\text{O}_3$  production rates are found to  
546 be similar for MOZART-4 and RADM2 chemistry (Figure 15). For both mechanisms, the greatest  
547 midday net  $\text{O}_3$  production rates are found in southern Europe, particularly over the Mediterranean  
548 and Atlantic coasts. The difference in net  $\text{O}_3$  production rate between the two mechanisms is also  
549 shown in Figure 15. MOZART exhibits greater net  $\text{O}_3$  photochemical production rates than RADM2  
550 for most of Europe, with the exception of the southeast corner of the domain (Greece, Turkey, and  
551 the nearby Mediterranean), where net  $\text{O}_3$  production rates are greater for RADM2. The difference  
552 in net  $\text{O}_3$  production rate (MOZART-RADM2) shows a large maximum over central Europe, cen-  
553 tering over Germany and extending west and east into France and Poland. Over Germany, net  $\text{O}_3$   
554 production in MOZART is seen to be higher than in RADM2 by  $1.8 \text{ ppb hr}^{-1}$  or more.

555 As expected, regions of high  $\text{NO}_2$  production in both MOZART and RADM2 simulations are seen  
556 over the high  $\text{NO}_x$ -emission regions including Benelux, southern England, western Germany, the  
557 Po Valley, and major cities including Paris and Moscow. The difference in net  $\text{NO}_2$  production rate  
558 between the two mechanisms is also highest where the absolute  $\text{NO}_2$  production rates are highest;  
559 in these areas the net  $\text{NO}_2$  production rate is lower for MOZART than for RADM2 by greater than  
560  $0.25 \text{ ppb hr}^{-1}$ . Furthermore, areas where the two mechanisms show the greatest differences in net

561 NO<sub>2</sub> production rate tend to be the areas where the net O<sub>3</sub> production rate is most different between  
562 the two mechanisms, including the large maximum over the Netherlands and northwest Germany.

563 To further investigate the differences between ozone chemistry in MOZART vs. RADM2, we  
564 performed two additional sensitivity studies with each mechanism: one in which all anthropogenic  
565 NO<sub>x</sub> emissions were increased by 30%, and one in which all anthropogenic VOC emissions were  
566 increased by 30%. We then examined the change in O<sub>3</sub> concentrations due to these emission per-  
567 turbations to diagnose whether the chemical mechanisms were operating in a NO<sub>x</sub>-sensitive or a  
568 VOC-sensitive regime. Results are shown in Figure 16. For the simulations where NO<sub>x</sub> emissions  
569 were increased by 30%, MOZART and RADM2 show very similar behavior. Most of the domain  
570 is NO<sub>x</sub> sensitive, with increased NO<sub>x</sub> emissions resulting in increased modeled O<sub>3</sub>. Notably, the  
571 U.K., Benelux, northern France and Paris, and northwest Germany show NO<sub>x</sub>-saturated behavior,  
572 in which increased NO<sub>x</sub> emissions lead to decreased O<sub>3</sub> concentrations. NO<sub>x</sub>-saturated regimes are  
573 also seen around the area of the Mediterranean between Monaco, Genoa and Corsica. An alternate  
574 approach to identify areas of NO<sub>x</sub>-sensitive vs. NO<sub>x</sub>-saturated regimes is to use indicator ratios (in  
575 the base simulation) following Sillman (1995). We have applied this approach with the indicator ratio  
576 CH<sub>2</sub>O/NO<sub>y</sub> (Figure S12) and find that areas identified as NO<sub>x</sub> sensitive using the indicator ratio are  
577 the same as those identified using the simulation with +30% NO<sub>x</sub> emissions. These results are also  
578 consistent with the areas of Europe found to be NO<sub>x</sub> saturated in the model study of Beekmann and  
579 Vautard (2010). Magnitudes of the observed change in O<sub>3</sub> in response to increased NO<sub>x</sub> emissions  
580 are quite similar for both mechanisms, although RADM2 shows slightly stronger NO<sub>x</sub> saturation  
581 (i.e., a stronger decrease in O<sub>3</sub> given a 30% increase in NO<sub>x</sub> emissions) in the area centered around  
582 Benelux, and stronger NO<sub>x</sub> sensitivity over Scandinavia and northwest Russia.

583 In contrast to the similar behavior seen for NO<sub>x</sub> sensitivity, the VOC sensitivity exhibited by the  
584 two mechanisms is quite different (Figure 16, lower panel). For both MOZART and RADM2, the  
585 effect of increased anthropogenic VOC emissions on O<sub>3</sub> is smaller than the effect of increased NO<sub>x</sub>  
586 emissions. The MOZART simulation shows very little impact of increased VOC emissions on O<sub>3</sub>,  
587 with differences in average O<sub>3</sub> concentration generally confined to ± 2% of the base simulation.  
588 In contrast, increasing VOC emissions in the RADM2 simulations leads to increased O<sub>3</sub> concentra-  
589 tions throughout nearly the entire domain. Areas where MOZART and RADM2 are in agreement in  
590 predicting VOC sensitivity (increased O<sub>3</sub> concentrations in response to increased VOC emissions)  
591 are generally those with high NO<sub>x</sub> emissions, where one would expect the highest VOC sensitivity  
592 based on theory; these areas include Benelux, northern France, northwest Germany, and shipping  
593 tracks in the Mediterranean. However, the increase in O<sub>3</sub> concentration is modest for both mecha-  
594 nisms; for RADM2 it is generally limited to increases of 2-4% over the base simulation. The results  
595 of the +30% VOC sensitivity studies for July indicate that d[O<sub>3</sub>]/d[VOC] is higher (more positive)  
596 for RADM2 than for MOZART for the chemical regime represented by the models in July 2007.  
597 This shows that the two mechanisms are simulating different O<sub>3</sub> chemical regimes – in the case of

598 RADM2, there is greater VOC sensitivity, meaning that addition of VOC emissions moves the chem-  
599 istry in the direction of maximum O<sub>3</sub> production efficiency; this is not the case for MOZART over  
600 much of the domain. A more extensive study would be needed to evaluate whether the conclusion  
601 that  $d[\text{O}_3]/d[\text{VOC}]$  is higher for RADM2 than for MOZART can be applied more generally.

602 Taken as a whole, Figure 16 shows that MOZART behaves in a classically NO<sub>x</sub>-sensitive manner  
603 for most of domain, with O<sub>3</sub> responding to changes in NO<sub>x</sub> but showing little response to changes  
604 in anthropogenic VOC. NO<sub>x</sub>-saturated behavior is also observed, particularly around the area of  
605 U.K., Benelux, and northern France and Germany. RADM2, on the other hand, exhibits more of  
606 a mixed NO<sub>x</sub>- VOC-sensitivity for much of the domain. The NO<sub>x</sub> sensitivity seen in RADM2 is  
607 very similar to that seen in MOZART, but the response of RADM2 to changes in VOC is much  
608 stronger (by about a factor of two) than observed in MOZART. With the exception of some small  
609 areas in the North and Baltic Sea south of Norway and Sweden, RADM2 predicts O<sub>3</sub> increases  
610 with VOC increases throughout the entire domain. This difference in VOC sensitivity seen between  
611 the mechanisms has implications for policy decisions, as it indicates uncertainty in the European  
612 response of O<sub>3</sub> to policies designed to reduce anthropogenic VOC emissions.

613 In addition to characterizing mechanism behavior with respect to net photochemical O<sub>3</sub> produc-  
614 tion and NO<sub>x</sub>- and VOC-sensitivity, we evaluate the contribution of other sources that could ex-  
615 plain the large differences in predicted O<sub>3</sub> between the MOZART and RADM2 simulations. First,  
616 MOZART and RADM2 use different rate coefficients for several inorganic gas phase chemical re-  
617 actions. To test the effect of these differences, all RADM2 inorganic reaction rate coefficients were  
618 changed so that they matched those used in MOZART simulations in the cases where the reactions  
619 are the same in both mechanisms (Section S3 in the Supplementary Material). The differences in  
620 inorganic rate coefficients between the two mechanisms explain a significant difference in predicted  
621 O<sub>3</sub> concentrations: when RADM2 is run with inorganic rate coefficients from MOZART, the result-  
622 ing domain-mean O<sub>3</sub> is higher by more than 8 μg m<sup>-3</sup> for the month of July, approximately 40% of  
623 the difference in predicted O<sub>3</sub>.

624 Besides the gas-phase chemistry itself, there are some differences in the implementation of MOZART-  
625 4 vs. RADM2 in WRF-Chem that could also contribute to the observed differences in modeled O<sub>3</sub>:  
626 in particular, in the treatment of dry deposition and photolysis (described in the Supplementary Ma-  
627 terial, Section S2). To test the effect of differences in treatment of dry deposition, we conducted  
628 an additional sensitivity in which we modified the RADM2 simulation to treat dry deposition in  
629 the same way as it is treated in MOZART. However, this led to only a small difference in average  
630 ozone (an increase of 1 μg m<sup>-3</sup>), indicating that modeled surface O<sub>3</sub> concentrations are relatively  
631 insensitive to these differences in the treatment of dry deposition, at least in the summer. In a sen-  
632 sitivity test where we modified the model code so that the MOZART simulation ran with the same  
633 photolysis scheme as used in our RADM2 simulation (i.e., with the Madronich TUV scheme and  
634 without reading in climatological O<sub>3</sub> and O<sub>2</sub> columns), we found that average O<sub>3</sub> for July decreases



635 by  $3 \mu\text{g m}^{-3}$ . This indicates that modeled  $\text{O}_3$  is also somewhat sensitive to differences in the treat-  
636 ment of photolysis in MOZART and RADM2. However, taken together, our sensitivity simulations  
637 suggest that the differences in the inorganic reaction rate coefficients are more important than the  
638 differing treatments of dry deposition and photolysis in explaining the differences in predicted  $\text{O}_3$   
639 between the RADM2 and MOZART simulations.

## 640 **5 Summary and Conclusions**

641 In this paper, we present a detailed description of a WRF-Chem setup over the European domain  
642 and provide an evaluation of the simulated meteorological and chemical fields with an emphasis  
643 on model's ability to reproduce the spatial and temporal distribution of ground-level  $\text{O}_3$  and  $\text{NO}_x$ .  
644 Within WRF-Chem we compare the performance of two different chemical mechanisms: MOZART-  
645 4, for which we present the first model evaluation for a European domain, and RADM2. Overall, we  
646 found that our WRF-Chem setup reproduced the spatial and seasonal variations in the meteorological  
647 parameters over Europe, with biases and correlations consistent with previous studies. Simulations  
648 using the MOZART- 4 as well as RADM2 chemical mechanisms were found to reproduce the spatial  
649 and temporal distributions in ground-level  $\text{O}_3$  over Europe, based on observations from the EMEP  
650 and Airbase networks. However, we find significant differences in  $\text{O}_3$  concentrations predicted by the  
651 two chemical mechanisms, with RADM2 predicting as much as  $20 \mu\text{g m}^{-3}$  less  $\text{O}_3$  than MOZART  
652 during the spring and summer seasons. In general, MOZART- 4 chemistry overpredicts  $\text{O}_3$  concen-  
653 trations for most of Europe in the summer and fall, whereas RADM2 leads to an underestimation of  
654  $\text{O}_3$  over the European domain in all seasons. Taken as a whole, use of MOZART- 4 chemistry per-  
655 forms better, leading to lower absolute model biases in  $\text{O}_3$ . This is the case when considering hourly  
656  $\text{O}_3$  concentrations as well as metrics relevant for human health, such as MDA8 and SOMO35. De-  
657 spite the large differences in predicted  $\text{O}_3$ , the two mechanisms show relatively similar behavior for  
658  $\text{NO}_x$ , with both MOZART and RADM2 simulations resulting in a slight underestimation of  $\text{NO}_x$   
659 compared to surface observations.

660 The net midday photochemical production rate of  $\text{O}_3$  in summer is found to be higher for MOZART  
661 than for RADM2 for most of the domain, with the largest differences between the mechanisms seen  
662 over Germany, where the net  $\text{O}_3$  photochemical production for MOZART is higher than for RADM2  
663 by greater than  $1.8 \text{ ppb hr}^{-1}$  ( $3.6 \mu\text{g m}^{-3} \text{ hr}^{-1}$ ). However, we have shown that RADM2 is approx-  
664 imately twice as sensitive to increases in anthropogenic VOC emissions as MOZART, suggesting  
665 that, under local VOC-limited conditions not seen at the regional scale of our simulations, RADM2  
666 is likely to produce  $\text{O}_3$  at a greater rate than MOZART. Despite the differences in sensitivity to  
667 changes in VOC emissions exhibited by the two mechanisms, sensitivity to changes in  $\text{NO}_x$  emis-  
668 sions in MOZART and RADM2 are found to be similar.

669 Our results indicate that modeled surface O<sub>3</sub> over Europe is sensitive the choice of gas phase  
670 chemical mechanism, with observed differences in O<sub>3</sub> between mechanisms that are larger than  
671 those seen in many past studies. Although the most fundamental differences between MOZART- 4  
672 and RADM2 (and other chemical mechanisms used in regional modeling) is the representation of  
673 VOC oxidation chemistry, we find that approximately 40% of the difference seen in predicted O<sub>3</sub>  
674 seen in this study can be explained by differences in inorganic reaction rate coefficients employed  
675 by MOZART- 4 and RADM2. **This result suggests that harmonization of inorganic rate coefficients  
676 among chemical mechanisms used for regional air quality modeling might be valuable, and could  
677 potentially lead to a smaller spread in model-predicted O<sub>3</sub> compared to that seen in, e.g., the multi-  
678 model studies of AQMEII (Solazzo et al., 2012b; Im et al., 2015).** Further investigation of chemical  
679 mechanism behavior within 3-D models in general would be helpful to constrain uncertainties in  
680 regional air quality modeling.

## 681 **6 Code availability**

682 The WRF-Chem model is an open-source, publicly available software. The code is being continually  
683 improved, with new releases approximately twice per year. WRF-Chem code can be downloaded at  
684 ([http://www2.mmm.ucar.edu/wrf/users/download/get\\_source.html](http://www2.mmm.ucar.edu/wrf/users/download/get_source.html)). The corresponding author will  
685 provide the bug fixes to version 3.5.1 used in this study, described in Section 2.3, upon request.

## 686 **Appendix A: Abbreviations and Acronyms**

687 DJF: December-January-February (winter)  
688 EDGAR: Emission Database for Global Atmospheric Research  
689 EEA: European Environmental Agency  
690 EOS: Earth Observing System  
691 GEOS5: Goddard Earth Observing System Model, Version 5  
692 GOCART: Goddard Chemistry Aerosol Radiation and Transport  
693 HTAP: Hemispheric Transport of Air Pollution  
694 JJA: June-July-August (summer)  
695 MADE: Modal Aerosol Dynamics Model for Europe  
696 MAM: March-April-May (spring)  
697 MERRA: Modern Era-Retrospective Analysis for Research and Applications  
698 NCEP: National Centers for Environmental Prediction  
699 NCAR: National Center for Atmospheric Research  
700 SON: September-October-November (fall)  
701 SORGAM: Secondary Organic Aerosol Model  
702 WRF-Chem: Weather Research and Forecasting with Chemistry

703 **Appendix B: Definitions of statistical quantities**

704 The statistical quantities used for model evaluation are defined below. Let  $Obs_i^j$  and  $Mod_i^j$  be the  
 705 observed and modeled quantities at time  $i$  and station  $j$ , respectively.  $N_{obs}^j$  represents the number of  
 706 temporal data points evaluated at station  $j$ , and  $N_{obs}$  represents the total number of data points (each  
 707 representing a time  $i$  and a station  $j$ ) evaluated in the domain.

708 The Mean Bias (MB) at a specific station (e.g., Figure 5) is calculated as

$$709 \quad MB^j = \frac{1}{N_{obs}^j} \sum_{i=1}^{N_{obs}^j} Mod_i^j - Obs_i^j$$

710 and the domain-wide Mean Bias (e.g., Table 5) as

$$711 \quad MB = \frac{1}{N_{obs}} \sum_{i,j=1}^{N_{obs}} Mod_i^j - Obs_i^j$$

712 Domain-wide values for Normalized Mean Bias (NMB) and Mean Fractional Bias (MFB) are  
 713 calculated analogously.

$$714 \quad NMB = \frac{\sum_{i=1}^{N_{obs}} Mod_i^j - Obs_i^j}{\sum_{i=1}^{N_{obs}} Obs_i^j}$$

$$715 \quad MFB = \frac{1}{N_{obs}} \sum_{i,j=1}^{N_{obs}} \frac{Mod_i^j - Obs_i^j}{\frac{Mod_i^j + Obs_i^j}{2}}$$

716 Temporal correlation between model results and observation is evaluated using the Pearson corre-  
 717 lation coefficient ( $r$ ). The value of  $r$  is calculated at each station using

$$718 \quad r^j = \frac{\sum_{i=1}^{N_{obs}^j} (Mod_i^j - \overline{Mod^j}) (Obs_i^j - \overline{Obs^j})}{\sigma_{mod} \times \sigma_{obs}}$$

719 Here, the numerator represents the covariance between the model and observations,  $\overline{Mod^j}$  and  
 720  $\overline{Obs^j}$  represent the mean of the model and observations, respectively, and  $\sigma$  is the standard deviation.

721 The domain-wide correlation coefficients (e.g., Table 5) is then calculated as

$$722 \quad r = \frac{1}{N_j} \sum_j r^j$$

723 where  $N_j$  is the total number of stations.

724 *Acknowledgements.* The authors would like to thank Renate Forkel for valuable discussions regarding the setup  
725 of our WRF-Chem simulation, and two anonymous reviewers for their feedback. The authors also thank Jane  
726 Coates for sharing her technique for VOC speciation and valuable discussions regarding chemical mecha-  
727 nisms. We thank TNO for access to the TNO-MACC II emissions inventory, and Hugo Denier van der Gon  
728 for helpful discussions regarding emissions. The HTAP v2.2 anthropogenic emissions were obtained from  
729 [http://edgar.jrc.ec.europa.eu/htap\\_v2/index.php](http://edgar.jrc.ec.europa.eu/htap_v2/index.php). The authors thank Christophe Knote and Anna Katinka Pe-  
730 tersen for sharing bug fixes for the WRF-Chem MOZART code. WRF-Chem tools for preprocessing bound-  
731 ary conditions as well as biogenic, fire, and anthropogenic emissions were provided by NCAR ([http://www.](http://www.acom.ucar.edu/wrf-chem/download.shtml)  
732 [acom.ucar.edu/wrf-chem/download.shtml](http://www.acom.ucar.edu/wrf-chem/download.shtml)). Initial and boundary conditions for meteorological fields were ob-  
733 tained from ECMWF, <http://www.ecmwf.int/en/research/climate-reanalysis/era-interim>. Initial and boundary  
734 conditions for chemical fields were from MOZART- 4/GEOS5, provided by NCAR at [http://www.acd.ucar.edu/](http://www.acd.ucar.edu/wrf-chem/mozart.shtml)  
735 [wrf-chem/mozart.shtml](http://www.acd.ucar.edu/wrf-chem/mozart.shtml). Corine land cover data was obtained from [http://www.eea.europa.eu/data-and-maps/](http://www.eea.europa.eu/data-and-maps/data/corine-land-cover-2006-raster-2)  
736 [data/corine-land-cover-2006-raster-2](http://www.eea.europa.eu/data-and-maps/data/corine-land-cover-2006-raster-2). We acknowledge the UK Met Office for providing the Global Weather  
737 Observation dataset via the British Atmospheric Data Centre. We acknowledge EMEP and the Norwegian In-  
738 stitute for Air Research (NILU) for providing the EMEP chemical observation data via the EBAS database  
739 ([ebas.nilu.no](http://ebas.nilu.no)). AirBase is the public air quality database of the EEA; data were obtained at [http://www.eea.](http://www.eea.europa.eu/data-and-maps/data/airbase-the-european-air-quality-database-7)  
740 [europa.eu/data-and-maps/data/airbase-the-european-air-quality-database-7](http://www.eea.europa.eu/data-and-maps/data/airbase-the-european-air-quality-database-7). The WRF-Chem simulations have  
741 been performed on the supercomputer HYDRA (<http://www.rzg.mpg.de/>).

## 742 References

- 743 Ackermann, I. J., Hass, H., Memmesheimer, M., Ebel, A., Binkowski, F. S., and Shankar, U.: Modal aerosol  
744 dynamics model for Europe: development and first applications, *Atmospheric Environment*, 32, 2981 –  
745 2999, doi:[http://dx.doi.org/10.1016/S1352-2310\(98\)00006-5](http://dx.doi.org/10.1016/S1352-2310(98)00006-5), [http://www.sciencedirect.com/science/article/  
746 pii/S1352231098000065](http://www.sciencedirect.com/science/article/pii/S1352231098000065), 1998a.
- 747 Ackermann, I. J., Hass, H., Memmesheimer, M., Ebel, A., Binkowski, F. S., and Shankar, U.: Modal aerosol  
748 dynamics model for Europe: development and first applications, *Atmospheric Environment*, 32, 2981 –  
749 2999, doi:[http://dx.doi.org/10.1016/S1352-2310\(98\)00006-5](http://dx.doi.org/10.1016/S1352-2310(98)00006-5), [http://www.sciencedirect.com/science/article/  
750 pii/S1352231098000065](http://www.sciencedirect.com/science/article/pii/S1352231098000065), 1998b.
- 751 Akritidis, D., Zanis, P., Katragkou, E., Schultz, M., Tegoulas, I., Poupkou, A., Markakis, K., Pytharoulis,  
752 I., and Karacostas, T.: Evaluating the impact of chemical boundary conditions on near surface  
753 ozone in regional climate–air quality simulations over Europe, *Atmospheric Research*, 134, 116 –  
754 130, doi:<http://dx.doi.org/10.1016/j.atmosres.2013.07.021>, [http://www.sciencedirect.com/science/article/pii/  
755 S0169809513002135](http://www.sciencedirect.com/science/article/pii/S0169809513002135), 2013.
- 756 Amann, M., Derwent, D., Forsberg, B., Hänninen, O., Hurley, F., Krzyzanowski, M., de Leeuw, F., Liu, S. J.,  
757 Mandin, C., Schneider, J., Schwarze, P., and Simpson, D.: Health risks of ozone from long-range transbound-  
758 ary air pollution, Tech. rep., World Health Organization Regional Office for Europe, 2008.
- 759 Andersson, E., Kahnert, M., and Devasthale, A.: Methodology for evaluating lateral boundary conditions in  
760 the regional chemical transport model MATCH (v5.5.0) using combined satellite and ground-based ob-  
761 servations, *Geoscientific Model Development*, 8, 3747–3763, doi:10.5194/gmd-8-3747-2015, [http://www.  
762 geosci-model-dev.net/8/3747/2015/](http://www.geosci-model-dev.net/8/3747/2015/), 2015.
- 763 Baklanov, A., Schlünzen, K., Suppan, P., Baldasano, J., Brunner, D., Aksoyoglu, S., Carmichael, G., Douros, J.,  
764 Flemming, J., Forkel, R., Galmarini, S., Gauss, M., Grell, G., Hirtl, M., Joffre, S., Jorba, O., Kaas, E., Kaasik,  
765 M., Kallos, G., Kong, X., Korsholm, U., Kurganskiy, A., Kushta, J., Lohmann, U., Mahura, A., Manders-  
766 Groot, A., Maurizi, A., Moussiopoulos, N., Rao, S. T., Savage, N., Seigneur, C., Sokhi, R. S., Solazzo,  
767 E., Solomos, S., Sørensen, B., Tsegas, G., Vignati, E., Vogel, B., and Zhang, Y.: Online coupled regional  
768 meteorology chemistry models in Europe: current status and prospects, *Atmospheric Chemistry and Physics*,  
769 14, 317–398, doi:10.5194/acp-14-317-2014, <http://www.atmos-chem-phys.net/14/317/2014/>, 2014.
- 770 Beekmann, M. and Vautard, R.: A modelling study of photochemical regimes over Europe: robustness and  
771 variability, *Atmospheric Chemistry and Physics*, 10, 10067–10084, doi:10.5194/acp-10-10067-2010, [http:  
772 //www.atmos-chem-phys.net/10/10067/2010/](http://www.atmos-chem-phys.net/10/10067/2010/), 2010.
- 773 Beljaars, A. C. M.: The parametrization of surface fluxes in large-scale models under free convection, *Quarterly*  
774 *Journal of the Royal Meteorological Society*, 121, 255–270, doi:10.1002/qj.49712152203, [http://dx.doi.org/  
775 10.1002/qj.49712152203](http://dx.doi.org/10.1002/qj.49712152203), 1995.
- 776 Bieser, J., Aulinger, A., Matthias, V., Quante, M., and Denier van der Gon, H.: Vertical emission  
777 profiles for Europe based on plume rise calculations, *Environmental Pollution*, 159, 2935–2946,  
778 doi:10.1016/j.envpol.2011.04.030, 2011.
- 779 Binkowski, F. S. and Shankar, U.: The Regional Particulate Matter Model: 1. Model description and preliminary  
780 results, *Journal of Geophysical Research: Atmospheres*, 100, 26191–26209, doi:10.1029/95JD02093, [http:  
781 //dx.doi.org/10.1029/95JD02093](http://dx.doi.org/10.1029/95JD02093), 1995.

782 Carter, W. P.: A detailed mechanism for the gas-phase atmospheric reactions of organic compounds, *At-*  
783 *mospheric Environment. Part A. General Topics*, 24, 481 – 518, doi:<http://dx.doi.org/10.1016/0960->  
784 [1686\(90\)90005-8](http://www.sciencedirect.com/science/article/pii/0960168690900058), <http://www.sciencedirect.com/science/article/pii/0960168690900058>, 1990.

785 Chen, F. and Dudhia, J.: Coupling and advanced land surface-hydrology model with the Penn State-NCAR  
786 MM5 modeling system, Part I: Model implementation and sensitivity, *Mon. Weather Rev.*, 129, 569–585,  
787 2001.

788 Chou, M.-D. and Suarez, M. J.: An efficient thermal infrared radiation parametrization for use in general circu-  
789 lation models, *NASA Tech. Memo.*, 104606, 85 pp., 1994.

790 Coates, J. and Butler, T. M.: A comparison of chemical mechanisms using tagged ozone production potential  
791 (TOPP) analysis, *Atmospheric Chemistry and Physics*, 15, 8795–8808, doi:10.5194/acp-15-8795-2015, [http:](http://www.atmos-chem-phys.net/15/8795/2015/)  
792 [//www.atmos-chem-phys.net/15/8795/2015/](http://www.atmos-chem-phys.net/15/8795/2015/), 2015.

793 Coates, J., Mar, K., Ojha, N., and Butler, T.: The Influence of Temperature on Ozone Production under vary-  
794 ing NO<sub>x</sub> Conditions – a modelling study, *Atmospheric Chemistry and Physics Discussions*, 2016, 1–18,  
795 doi:10.5194/acp-2016-260, <http://www.atmos-chem-phys-discuss.net/acp-2016-260/>, 2016.

796 Damian, V., Sandu, A., Damian, M., Potra, F., and Carmichael, G. R.: The kinetic preprocessor KPP-a  
797 software environment for solving chemical kinetics, *Computers & Chemical Engineering*, 26, 1567 –  
798 1579, doi:[http://dx.doi.org/10.1016/S0098-1354\(02\)00128-X](http://dx.doi.org/10.1016/S0098-1354(02)00128-X), [http://www.sciencedirect.com/science/article/](http://www.sciencedirect.com/science/article/pii/S009813540200128X)  
799 [pii/S009813540200128X](http://www.sciencedirect.com/science/article/pii/S009813540200128X), 2002.

800 Denier van der Gon, H., Hendriks, C., Kuenen, J., Segers, A., and Visschedijk, A.: Description of current  
801 temporal emission patterns and sensitivity of predicted AQ for temporal emission patterns, TNO report, EU  
802 FP7 MACC deliverable report D\_D-EMIS\_1.3, 2011.

803 EEA: Corine Land Cover 2006 raster data, Copenhagen, Denmark, doi:accessed June 2015, [http://www.eea.](http://www.eea.europa.eu/data-and-maps/data/corine-land-cover-2006-raster-2)  
804 [europa.eu/data-and-maps/data/corine-land-cover-2006-raster-2](http://www.eea.europa.eu/data-and-maps/data/corine-land-cover-2006-raster-2), 2012.

805 EEA: Air quality in Europe - 2014 report, Tech. Rep. 5/2014, European Environmental Agency,  
806 doi:10.2800/22847, 2014.

807 Emmons, L. K., Walters, S., Hess, P. G., Lamarque, J.-F., Pfister, G. G., Fillmore, D., Granier, C., Guenther, A.,  
808 Kinnison, D., Laepple, T., Orlando, J., Tie, X., Tyndall, G., Wiedinmyer, C., Baughcum, S. L., and Kloster, S.:  
809 Description and evaluation of the Model for Ozone and Related chemical Tracers, version 4 (MOZART-4),  
810 *Geoscientific Model Development*, 3, 43–67, doi:10.5194/gmd-3-43-2010, [http://www.geosci-model-dev.](http://www.geosci-model-dev.net/3/43/2010/)  
811 [net/3/43/2010/](http://www.geosci-model-dev.net/3/43/2010/), 2010.

812 Faraji, M., Kimura, Y., McDonald-Buller, E., and Allen, D.: Comparison of the carbon bond and {SAPRC}  
813 photochemical mechanisms under conditions relevant to southeast Texas, *Atmospheric Environment*, 42,  
814 5821 – 5836, doi:<http://dx.doi.org/10.1016/j.atmosenv.2007.07.048>, [http://www.sciencedirect.com/science/](http://www.sciencedirect.com/science/article/pii/S1352231007006565)  
815 [article/pii/S1352231007006565](http://www.sciencedirect.com/science/article/pii/S1352231007006565), selected Papers from the First International Conference on Atmospheric  
816 Chemical Mechanisms, 2008.

817 Forkel, R., Werhahn, J., Hansen, A. B., McKeen, S., Peckham, S., Grell, G., and Suppan, P.: Effect of aerosol-  
818 radiation feedback on regional air quality – A case study with WRF/Chem, *Atmospheric Environment*,  
819 53, 202 – 211, doi:<http://dx.doi.org/10.1016/j.atmosenv.2011.10.009>, [http://www.sciencedirect.com/science/](http://www.sciencedirect.com/science/article/pii/S1352231011010545)  
820 [article/pii/S1352231011010545](http://www.sciencedirect.com/science/article/pii/S1352231011010545), aQMEII: An International Initiative for the Evaluation of Regional-Scale  
821 Air Quality Models - Phase 1, 2012.

822 Forkel, R., Balzarini, A., Baró, R., Bianconi, R., Curci, G., Jiménez-Guerrero, P., Hirtl, M., Hon-  
823 zak, L., Lorenz, C., Im, U., Pérez, J. L., Pirovano, G., José, R. S., Tuccella, P., Werhahn, J., and  
824 Žabkar, R.: Analysis of the WRF-Chem contributions to {AQMEII} phase2 with respect to aerosol  
825 radiative feedbacks on meteorology and pollutant distributions, *Atmospheric Environment*, 115, 630  
826 – 645, doi:<http://dx.doi.org/10.1016/j.atmosenv.2014.10.056>, [http://www.sciencedirect.com/science/article/  
827 pii/S135223101400853X](http://www.sciencedirect.com/science/article/pii/S135223101400853X), 2015.

828 Geiger, H., Barnes, I., Bejan, I., Benter, T., and Spittler, M.: The tropospheric degradation of isoprene: an  
829 updated module for the regional atmospheric chemistry mechanism, *Atmospheric Environment*, 37, 1503 –  
830 1519, doi:[http://dx.doi.org/10.1016/S1352-2310\(02\)01047-6](http://dx.doi.org/10.1016/S1352-2310(02)01047-6), [http://www.sciencedirect.com/science/article/  
831 pii/S1352231002010476](http://www.sciencedirect.com/science/article/pii/S1352231002010476), 2003.

832 Gery, M. W., Whitten, G. Z., Killus, J. P., and Dodge, M. C.: A photochemical kinetics mechanism for urban  
833 and regional scale computer modeling, *Journal of Geophysical Research: Atmospheres*, 94, 12 925–12 956,  
834 doi:[10.1029/JD094iD10p12925](https://doi.org/10.1029/JD094iD10p12925), <http://dx.doi.org/10.1029/JD094iD10p12925>, 1989.

835 Grell, G. A. and Dévényi, D.: A generalized approach to parameterizing convection combining ensemble and  
836 data assimilation techniques, *Geophysical Research Letters*, 29, 38–1–38–4, doi:[10.1029/2002GL015311](https://doi.org/10.1029/2002GL015311),  
837 <http://dx.doi.org/10.1029/2002GL015311>, 2002.

838 Grell, G. A., Knoche, R., Peckham, S. E., and McKeen, S. A.: Online versus offline air quality modeling  
839 on cloud-resolving scales, *Geophysical Research Letters*, 31, n/a–n/a, doi:[10.1029/2004GL020175](https://doi.org/10.1029/2004GL020175), [http://  
840 dx.doi.org/10.1029/2004GL020175](http://dx.doi.org/10.1029/2004GL020175), 116117, 2004.

841 Grell, G. A., Peckham, S. E., Schmitz, R., McKeen, S. A., Frost, G., Skamarock, W. C., and  
842 Eder, B.: Fully coupled “online” chemistry within the WRF model, *Atmospheric Environment*, 39,  
843 doi:[10.1016/j.atmosenv.2005.04.027](https://doi.org/10.1016/j.atmosenv.2005.04.027), <http://dx.doi.org/10.1016/j.atmosenv.2005.04.027>, 2005.

844 Guenther, A., Karl, T., Harley, P., Wiedinmyer, C., Palmer, P. I., and Geron, C.: Estimates of global terrestrial  
845 isoprene emissions using MEGAN (Model of Emissions of Gases and Aerosols from Nature), *Atmospheric  
846 Chemistry and Physics*, 6, 3181–3210, doi:[10.5194/acp-6-3181-2006](https://doi.org/10.5194/acp-6-3181-2006), [http://www.atmos-chem-phys.net/6/  
847 3181/2006/](http://www.atmos-chem-phys.net/6/3181/2006/), 2006.

848 Hong, S.-Y., Noh, Y., and Dudhia, J.: A New Vertical Diffusion Package with an Explicit Treatment of Entrain-  
849 ment Processes, *Monthly Weather Review*, 134, 2318–2341, <http://dx.doi.org/10.1175/MWR3199.1>, doi:  
850 10.1175/MWR3199.1, 2006.

851 Iacono, M. J., Delamere, J. S., Mlawer, E. J., Shephard, M. W., Clough, S. A., and Collins, W. D.: Radiative  
852 forcing by long-lived greenhouse gases: Calculations with the AER radiative transfer models, *Journal of  
853 Geophysical Research: Atmospheres*, 113, n/a–n/a, doi:[10.1029/2008JD009944](https://doi.org/10.1029/2008JD009944), [http://dx.doi.org/10.1029/  
854 2008JD009944](http://dx.doi.org/10.1029/2008JD009944), d13103, 2008.

855 Im, U., Bianconi, R., Solazzo, E., Kioutsioukis, I., Badia, A., Balzarini, A., Baró, R., Bellasio, R., Brun-  
856 ner, D., Chemel, C., Curci, G., Flemming, J., Forkel, R., Giordano, L., Jiménez-Guerrero, P., Hirtl, M.,  
857 Hodzic, A., Honzak, L., Jorba, O., Knote, C., Kuenen, J. J., Makar, P. A., Manders-Groot, A., Neal, L.,  
858 Pérez, J. L., Pirovano, G., Pouliot, G., Jose, R. S., Savage, N., Schroder, W., Sokhi, R. S., Syrakov, D.,  
859 Torian, A., Tuccella, P., Werhahn, J., Wolke, R., Yahya, K., Zabkar, R., Zhang, Y., Zhang, J., Hogrefe, C.,  
860 and Galmarini, S.: Evaluation of operational on-line-coupled regional air quality models over Europe and  
861 North America in the context of {AQMEII} phase 2. Part I: Ozone, *Atmospheric Environment*, 115, 404

862 – 420, doi:<http://dx.doi.org/10.1016/j.atmosenv.2014.09.042>, <http://www.sciencedirect.com/science/article/pii/S1352231014007353>, 2015.

864 Janssens-Maenhout, G., Crippa, M., Guizzardi, D., Dentener, F., Muntean, M., Pouliot, G., Keating, T., Zhang,  
865 Q., Kurokawa, J., Wankmüller, R., Denier van der Gon, H., Klimont, Z., Frost, G., Darras, S., and Koffi, B.:  
866 HTAP v2: a mosaic of regional and global emission gridmaps for 2008 and 2010 to study hemispheric trans-  
867 port of air pollution, *Atmospheric Chemistry and Physics Discussions*, 15, 12 867–12 909, doi:10.5194/acpd-  
868 15-12867-2015, <http://www.atmos-chem-phys-discuss.net/15/12867/2015/>, 2015.

869 Kim, Y., Sartelet, K., and Seigneur, C.: Comparison of two gas-phase chemical kinetic mechanisms of ozone  
870 formation over Europe, *Journal of Atmospheric Chemistry*, 62, 89–119, doi:10.1007/s10874-009-9142-5,  
871 <http://dx.doi.org/10.1007/s10874-009-9142-5>, 2010.

872 Knote, C., Tuccella, P., Curci, G., Emmons, L., Orlando, J. J., Madronich, S., Baró, R., Jiménez-Guerrero,  
873 P., Luecken, D., Hogrefe, C., Forkel, R., Werhahn, J., Hirtl, M., Pérez, J. L., José, R. S., Giordano, L.,  
874 Brunner, D., Yahya, K., and Zhang, Y.: Influence of the choice of gas-phase mechanism on predictions of  
875 key gaseous pollutants during the {AQMEII} phase-2 intercomparison, *Atmospheric Environment*, 115, 553  
876 – 568, doi:<http://dx.doi.org/10.1016/j.atmosenv.2014.11.066>, <http://www.sciencedirect.com/science/article/pii/S1352231014009388>, 2015.

878 Kuenen, J., Visschedijk, J., Jozwicka, M., and Denier van der Gon, H.: TNO-MACC\_II emission inven-  
879 tory: a multi-year (2003-2009) consistent high-resolution European inventory for air quality modelling,  
880 *Atmospheric Chemistry and Physics*, 14, 10 963–10 976, doi:10.5194/acp-14-10963-2014, [http://www.](http://www.atmos-chem-phys.net/14/10963/2014/)  
881 [atmos-chem-phys.net/14/10963/2014/](http://www.atmos-chem-phys.net/14/10963/2014/), 2014.

882 Kuik, F., Lauer, A., Churkina, G., Denier van der Gon, H. A. C., Fenner, D., Mar, K. A., and Butler, T. M.:  
883 Air quality modelling in the Berlin-Brandenburg region using WRF-Chem v3.7.1: sensitivity to resolution  
884 of model grid and input data, *Geoscientific Model Development Discussions*, 2016, 1–46, doi:10.5194/gmd-  
885 2016-190, <http://www.geosci-model-dev-discuss.net/gmd-2016-190/>, 2016.

886 Kusaka, H. and Kimura, F.: Thermal Effects of Urban Canyon Structure on the Nocturnal Heat Island: Nu-  
887 merical Experiment Using a Mesoscale Model Coupled with an Urban Canopy Model, *Journal of Applied*  
888 *Meteorology*, 43, 1899–1910, <http://dx.doi.org/10.1175/JAM2169.1>, doi: 10.1175/JAM2169.1, 2004.

889 Lelieveld, J., Evans, J. S., Fnais, M., Giannadaki, D., and Pozzer, A.: The contribution of outdoor air pol-  
890 lution sources to premature mortality on a global scale, *Nature*, 525, 367–371, [http://dx.doi.org/10.1038/](http://dx.doi.org/10.1038/nature15371)  
891 [nature15371](http://dx.doi.org/10.1038/nature15371), letter, 2015.

892 Lin, Y.-L., Farley, R. D., and Orville, H. D.: Bulk Parameterization of the Snow Field in a  
893 Cloud Model, *Journal of Climate and Applied Meteorology*, 22, 1065–1092, doi:10.1175/1520-  
894 0450(1983)022<1065:BPOTSF>2.0.CO;2, [http://dx.doi.org/10.1175/1520-0450\(1983\)022<1065:](http://dx.doi.org/10.1175/1520-0450(1983)022<1065:BPOTSF>2.0.CO;2)  
895 [BPOTSF>2.0.CO;2](http://dx.doi.org/10.1175/1520-0450(1983)022<1065:BPOTSF>2.0.CO;2), 1983.

896 Liu, P., Tsimpidi, A. P., Hu, Y., Stone, B., Russell, A. G., and Nenes, A.: Differences between downscaling with  
897 spectral and grid nudging using WRF, *Atmospheric Chemistry and Physics*, 12, 3601–3610, doi:10.5194/acp-  
898 12-3601-2012, <http://www.atmos-chem-phys.net/12/3601/2012/>, 2012.

899 Luecken, D., Phillips, S., Sarwar, G., and Jang, C.: Effects of using the {CB05} vs. {SAPRC99} vs. {CB4}  
900 chemical mechanism on model predictions: Ozone and gas-phase photochemical precursor concentrations,  
901 *Atmospheric Environment*, 42, 5805 – 5820, doi:<http://dx.doi.org/10.1016/j.atmosenv.2007.08.056>, <http://>



902 [www.sciencedirect.com/science/article/pii/S1352231007007728](http://www.sciencedirect.com/science/article/pii/S1352231007007728), selected Papers from the First International  
903 Conference on Atmospheric Chemical Mechanisms, 2008.

904 Mallet, V. and Sportisse, B.: Uncertainty in a chemistry-transport model due to physical parameterizations and  
905 numerical approximations: An ensemble approach applied to ozone modeling, *Journal of Geophysical Re-*  
906 *search: Atmospheres*, 111, n/a–n/a, doi:10.1029/2005JD006149, <http://dx.doi.org/10.1029/2005JD006149>,  
907 d01302, 2006.

908 Mallet, V., Quélo, D., Sportisse, B., Ahmed de Biasi, M., Debry, E., Korsakissok, I., Wu, L., Rous-  
909 tan, Y., Sartelet, K., Tombette, M., and Foudhil, H.: Technical Note: The air quality modeling sys-  
910 tem Polyphemus, *Atmospheric Chemistry and Physics*, 7, 5479–5487, doi:10.5194/acp-7-5479-2007, [http://](http://www.atmos-chem-phys.net/7/5479/2007/)  
911 [www.atmos-chem-phys.net/7/5479/2007/](http://www.atmos-chem-phys.net/7/5479/2007/), 2007.

912 Miguez-Macho, G., Stenchikov, G., and Robock, A.: Spectral nudging to eliminate the effects of domain po-  
913 sition and geometry in regional climate model simulations, *Journal of Geophysical Research: Atmospheres*,  
914 109, doi:10.1029/2003JD004495, 2004.

915 Monks, P. S., Archibald, A. T., Colette, A., Cooper, O., Coyle, M., Derwent, R., Fowler, D., Granier, C., Law,  
916 K. S., Mills, G. E., Stevenson, D. S., Tarasova, O., Thouret, V., von Schneidemesser, E., Sommariva, R., Wild,  
917 O., and Williams, M. L.: Tropospheric ozone and its precursors from the urban to the global scale from air  
918 quality to short-lived climate forcer, *Atmospheric Chemistry and Physics*, 15, 8889–8973, doi:10.5194/acp-  
919 15-8889-2015, <http://www.atmos-chem-phys.net/15/8889/2015/>, 2015.

920 Pfister, G. G., Walters, S., Emmons, L. K., Edwards, D. P., and Avise, J.: Quantifying the contribution  
921 of inflow on surface ozone over California during summer 2008, *Journal of Geophysical Research:*  
922 *Atmospheres*, 118, 12,282–12,299, doi:10.1002/2013JD020336, <http://dx.doi.org/10.1002/2013JD020336>,  
923 2013JD020336, 2013.

924 Sandu, A. and Sander, R.: Technical note: Simulating chemical systems in Fortran90 and Matlab with the  
925 Kinetic PreProcessor KPP-2.1, *Atmospheric Chemistry and Physics*, 6, 187–195, doi:10.5194/acp-6-187-  
926 2006, <http://www.atmos-chem-phys.net/6/187/2006/>, 2006.

927 Schaap, M., Roemer, M., Sauter, F., Boersen, G., Timmermans, R., and Bultjes, P.: LOTOS-EUROS: Docu-  
928 mentation, TNO report B&O-A, 2005.

929 Schaap, M., Timmermans, R., Roemer, M., Boersen, G., Bultjes, P., Sauter, F., Velders, G., and Beck,  
930 J.: The LOTOS-EUROS model: Description, validation and latest developments, *International Journal of*  
931 *Environment and Pollution*, 32, 270–290, doi:10.1504/IJEP.2008.017106, [http://www.scopus.com/inward/](http://www.scopus.com/inward/record.url?eid=2-s2.0-39349101242&partnerID=40&md5=af80f203e8a045cbb128dc3b58074135)  
932 [record.url?eid=2-s2.0-39349101242&partnerID=40&md5=af80f203e8a045cbb128dc3b58074135](http://www.scopus.com/inward/record.url?eid=2-s2.0-39349101242&partnerID=40&md5=af80f203e8a045cbb128dc3b58074135), cited By  
933 0, 2008.

934 Schell, B., Ackermann, I. J., Hass, H., Binkowski, F. S., and Ebel, A.: Modeling the formation of secondary  
935 organic aerosol within a comprehensive air quality model system, *Journal of Geophysical Research: Atmo-*  
936 *spheres*, 106, 28 275–28 293, doi:10.1029/2001JD000384, <http://dx.doi.org/10.1029/2001JD000384>, 2001.

937 Sillman, S.: The use of NO<sub>y</sub>, H<sub>2</sub>O<sub>2</sub>, and HNO<sub>3</sub> as indicators for ozone-NO<sub>x</sub>-hydrocarbon sensitivity in ur-  
938 ban locations, *Journal of Geophysical Research: Atmospheres*, 100, 14 175–14 188, doi:10.1029/94JD02953,  
939 <http://dx.doi.org/10.1029/94JD02953>, 1995.

940 Simpson, D., Benedictow, A., Berge, H., Bergström, R., Emberson, L. D., Fagerli, H., Flechard, C. R.,  
941 Hayman, G. D., Gauss, M., Jonson, J. E., Jenkin, M. E., Nyíri, A., Richter, C., Semeena, V. S., Tsyro,

942 S., Tuovinen, J.-P., Valdebenito, A., and Wind, P.: The EMEP MSC-W chemical transport model –tech-  
943 nical description, *Atmospheric Chemistry and Physics*, 12, 7825–7865, doi:10.5194/acp-12-7825-2012,  
944 <http://www.atmos-chem-phys.net/12/7825/2012/>, 2012.

945 Solazzo, E., Bianconi, R., Pirovano, G., Matthias, V., Vautard, R., Moran, M. D., Appel, K. W., Bessagnet,  
946 B., Brandt, J., Christensen, J. H., Chemel, C., Coll, I., Ferreira, J., Forkel, R., Francis, X. V., Grell, G.,  
947 Grossi, P., Hansen, A. B., Miranda, A. I., Nopmongcol, U., Prank, M., Sartelet, K. N., Schaap, M., Silver,  
948 J. D., Sokhi, R. S., Vira, J., Werhahn, J., Wolke, R., Yarwood, G., Zhang, J., Rao, S. T., and Galmarini,  
949 S.: Operational model evaluation for particulate matter in Europe and North America in the context of  
950 {AQMEII}, *Atmospheric Environment*, 53, 75 – 92, doi:<http://dx.doi.org/10.1016/j.atmosenv.2012.02.045>,  
951 <http://www.sciencedirect.com/science/article/pii/S1352231012001604>, aQMEII: An International Initiative  
952 for the Evaluation of Regional-Scale Air Quality Models - Phase 1, 2012a.

953 Solazzo, E., Bianconi, R., Vautard, R., Appel, K. W., Moran, M. D., Hogrefe, C., Bessagnet, B., Brandt, J.,  
954 Christensen, J. H., Chemel, C., Coll, I., van der Gon, H. D., Ferreira, J., Forkel, R., Francis, X. V., Grell,  
955 G., Grossi, P., Hansen, A. B., Jeričević, A., Kraljević, L., Miranda, A. I., Nopmongcol, U., Pirovano, G.,  
956 Prank, M., Riccio, A., Sartelet, K. N., Schaap, M., Silver, J. D., Sokhi, R. S., Vira, J., Werhahn, J., Wolke, R.,  
957 Yarwood, G., Zhang, J., Rao, S., and Galmarini, S.: Model evaluation and ensemble modelling of surface-  
958 level ozone in Europe and North America in the context of {AQMEII}, *Atmospheric Environment*, 53, 60 –  
959 74, doi:<http://dx.doi.org/10.1016/j.atmosenv.2012.01.003>, <http://www.sciencedirect.com/science/article/pii/S1352231012000064>, aQMEII: An International Initiative for the Evaluation of Regional-Scale Air Quality  
960 Models - Phase 1, 2012b.

961  
962 Stauffer, D. R., Seaman, N. L., and Binkowski, F. S.: Use of Four-Dimensional Data Assimilation in a Limited-  
963 Area Mesoscale Model Part II: Effects of Data Assimilation within the Planetary Boundary Layer, *Mon.*  
964 *Wea. Rev.*, 119, 734–754, doi:10.1175/1520-0493(1991)119<0734:UOFDDA>2.0.CO;2, [http://dx.doi.org/](http://dx.doi.org/10.1175/1520-0493(1991)119<0734:UOFDDA>2.0.CO;2)  
965 [10.1175/1520-0493\(1991\)119<0734:UOFDDA>2.0.CO;2](http://dx.doi.org/10.1175/1520-0493(1991)119<0734:UOFDDA>2.0.CO;2), 1991.

966 Stegehuis, A., Vautard, R., Ciais, P., Teuling, A., Miralles, D., and Wild., M.: An observation-constrained multi-  
967 physics RCM ensemble for simulating European mega-heatwaves, *Geoscientific Model Development Dis-*  
968 *cussions*, 7, 7861–7886, doi:10.5194/gmdd-7-7861-2014, 2014.

969 Stevenson, D. S., Young, P. J., Naik, V., Lamarque, J.-F., Shindell, D. T., Voulgarakis, A., Skeie, R. B., Dal-  
970 soren, S. B., Myhre, G., Berntsen, T. K., Folberth, G. A., Rumbold, S. T., Collins, W. J., MacKenzie, I. A.,  
971 Doherty, R. M., Zeng, G., van Noije, T. P. C., Strunk, A., Bergmann, D., Cameron-Smith, P., Plummer, D. A.,  
972 Strode, S. A., Horowitz, L., Lee, Y. H., Szopa, S., Sudo, K., Nagashima, T., Josse, B., Cionni, I., Righi, M.,  
973 Eyring, V., Conley, A., Bowman, K. W., Wild, O., and Archibald, A.: Tropospheric ozone changes, radia-  
974 tive forcing and attribution to emissions in the Atmospheric Chemistry and Climate Model Intercomparison  
975 Project (ACCMIP), *Atmospheric Chemistry and Physics*, 13, 3063–3085, doi:10.5194/acp-13-3063-2013,  
976 <http://www.atmos-chem-phys.net/13/3063/2013/>, 2013.

977 Stockwell, W. R., Middleton, P., Chang, J. S., and Tang, X.: The second generation regional acid deposition  
978 model chemical mechanism for regional air quality modeling, *Journal of Geophysical Research: Atmo-*  
979 *spheres*, 95, 16 343–16 367, doi:10.1029/JD095iD10p16343, <http://dx.doi.org/10.1029/JD095iD10p16343>,  
980 1990.

981 Stockwell, W. R., Kirchner, F., Kuhn, M., and Seefeld, S.: A new mechanism for regional atmospheric chemistry  
982 modeling, *Journal of Geophysical Research: Atmospheres*, 102, 25 847–25 879, doi:10.1029/97JD00849,  
983 <http://dx.doi.org/10.1029/97JD00849>, 1997.

984 Terrenoire, E., Bessagnet, B., Rouïl, L., Tognet, F., Pirovano, G., Létinois, L., Beauchamp, M., Colette, A.,  
985 Thunis, P., Amann, M., and Menut, L.: High-resolution air quality simulation over Europe with the chemistry  
986 transport model CHIMERE, *Geoscientific Model Development*, 8, 21–42, doi:10.5194/gmd-8-21-2015, <http://www.geosci-model-dev.net/8/21/2015/>, 2015.

988 Tørseth, K., Aas, W., Breivik, K., Fjæraa, A. M., Fiebig, M., Hjellbrekke, A. G., Lund Myhre, C., Solberg, S.,  
989 and Yttri, K. E.: Introduction to the European Monitoring and Evaluation Programme (EMEP) and observed  
990 atmospheric composition change during 1972–2009, *Atmospheric Chemistry and Physics*, 12, 5447–5481,  
991 doi:10.5194/acp-12-5447-2012, <http://www.atmos-chem-phys.net/12/5447/2012/>, 2012.

992 Tuccella, P., Curci, G., Visconti, G., Bessagnet, B., Menut, L., and Park, R. J.: Modeling of gas and aerosol with  
993 WRF/Chem over Europe: Evaluation and sensitivity study, *Journal of Geophysical Research: Atmospheres*,  
994 117, n/a–n/a, doi:10.1029/2011JD016302, <http://dx.doi.org/10.1029/2011JD016302>, d03303, 2012.

995 von Schneidmesser, E., Coates, J., van der Gon, H. D., Visschedijk, A., and Butler, T.: Variation of the  
996 {NMVOC} speciation in the solvent sector and the sensitivity of modelled tropospheric ozone, *Atmospheric  
997 Environment*, 135, 59 – 72, doi:<http://dx.doi.org/10.1016/j.atmosenv.2016.03.057>, <http://www.sciencedirect.com/science/article/pii/S1352231016302242>, 2016.

999 Žabkar, R., Honzak, L., Skok, G., Forkel, R., Rakovec, J., Ceglar, A., and Žagar, N.: Evaluation of the high reso-  
1000 lution WRF-Chem (v3.4.1) air quality forecast and its comparison with statistical ozone predictions, *Geosci-  
1001 entific Model Development*, 8, 2119–2137, doi:10.5194/gmd-8-2119-2015, <http://www.geosci-model-dev.net/8/2119/2015/>, 2015.

1003 Wang, W., Bruyère, C., Duda, M., Dudhia, J., Gill, D., Kavulich, M., Keene, K., Lin, H.-C., Michalakes, J.,  
1004 Rizvi, S., and Zhang, X.: ARW Version 3 Modeling System User’s Guide, Chapter 3: WRF Preprocessing  
1005 System (WPS), pp. 59–60, 2014.

1006 WHO: Health Aspects of Air Pollution with Particulate Matter, Ozone and Nitrogen Dioxide, Bonn, 2003.

1007 WHO, R. O. f. E.: Review of evidence on health aspects of air pollution – REVIHAAP Project, Tech. rep.,  
1008 World Health Organization, 2013.

1009 Wiedinmyer, C., Akagi, S. K., Yokelson, R. J., Emmons, L. K., Al-Saadi, J. A., Orlando, J. J., and Soja, A. J.:  
1010 The Fire INventory from NCAR (FINN): a high resolution global model to estimate the emissions from  
1011 open burning, *Geoscientific Model Development*, 4, 625–641, doi:10.5194/gmd-4-625-2011, <http://www.geosci-model-dev.net/4/625/2011/>, 2011.

1013 Wilson, R. C., Fleming, Z. L., Monks, P. S., Clain, G., Henne, S., Kononov, I. B., Szopa, S., and Menut, L.:  
1014 Have primary emission reduction measures reduced ozone across Europe? An analysis of European rural  
1015 background ozone trends 1996–2005, *Atmospheric Chemistry and Physics*, 12, 437–454, doi:10.5194/acp-  
1016 12-437-2012, <http://www.atmos-chem-phys.net/12/437/2012/>, 2012.

1017 Yarwood, G., Stoeckenius, T. E., Heiken, J. G., and Dunker, A. M.: Modeling Weekday/Weekend Ozone Dif-  
1018 ferences in the Los Angeles Region for 1997, *Journal of the Air & Waste Management Association*, 53, 864–  
1019 875, doi:10.1080/10473289.2003.10466232, <http://dx.doi.org/10.1080/10473289.2003.10466232>, 2003.

1020 Yarwood, G., Rao, S., Yocke, M., and Whitten, G. Z.: Updates to the Carbon Bond Chemical Mechanism:  
1021 CB05, Tech. rep., U. S Environmental Protection Agency, 2005.

1022 Zaveri, R. A. and Peters, L. K.: A new lumped structure photochemical mechanism for large-scale applications,  
1023 Journal of Geophysical Research: Atmospheres, 104, 30 387–30 415, doi:10.1029/1999JD900876, [http://dx.  
doi.org/10.1029/1999JD900876](http://dx.<br/>1024 doi.org/10.1029/1999JD900876), 1999.

1025 Zhang, Y.: Online-coupled meteorology and chemistry models: history, current status, and outlook, Atmo-  
1026 spheric Chemistry and Physics, 8, 2895–2932, doi:10.5194/acp-8-2895-2008, [http://www.atmos-chem-phys.  
net/8/2895/2008/](http://www.atmos-chem-phys.<br/>1027 net/8/2895/2008/), 2008.

1028 Zhang, Y., Pan, Y., Wang, K., Fast, J. D., and Grell, G. A.: WRF/Chem-MADRID: Incorporation of an aerosol  
1029 module into WRF/Chem and its initial application to the TexAQS2000 episode, Journal of Geophysical Re-  
1030 search: Atmospheres, 115, n/a–n/a, doi:10.1029/2009JD013443, [http://dx.doi.org/10.1029/2009JD013443,  
d18202](http://dx.doi.org/10.1029/2009JD013443,<br/>1031 d18202), 2010.

1032 Zhang, Y., Chen, Y., Sarwar, G., and Schere, K.: Impact of gas-phase mechanisms on Weather Research  
1033 Forecasting Model with Chemistry (WRF/Chem) predictions: Mechanism implementation and compara-  
1034 tive evaluation, Journal of Geophysical Research: Atmospheres, 117, n/a–n/a, doi:10.1029/2011JD015775,  
1035 <http://dx.doi.org/10.1029/2011JD015775>, d01301, 2012.

1036 Zhang, Y., Sartelet, K., Wu, S.-Y., and Seigneur, C.: Application of WRFChem-MADRID and WRFPolyphemus  
1037 in Europe – Part 1: Model description, evaluation of meteorological predictions, and aerosol–meteorology  
1038 interactions, Atmospheric Chemistry and Physics, 13, 6807–6843, doi:10.5194/acp-13-6807-2013, [http://  
www.atmos-chem-phys.net/13/6807/2013/](http://<br/>1039 www.atmos-chem-phys.net/13/6807/2013/), 2013a.

1040 Zhang, Y., Sartelet, K., Zhu, S., Wang, W., Wu, S.-Y., Zhang, X., Wang, K., Tran, P., Seigneur, C., and  
1041 Wang, Z.-F.: Application of WRF/Chem-MADRID and WRF/Polyphemus in Europe – Part 2: Evaluation of  
1042 chemical concentrations and sensitivity simulations, Atmospheric Chemistry and Physics, 13, 6845–6875,  
1043 doi:10.5194/acp-13-6845-2013, <http://www.atmos-chem-phys.net/13/6845/2013/>, 2013b.

**Table 1.** WRF-Chem options used in model simulations.

Atmospheric Process	Option used
Cloud microphysics	Lin et al. scheme (Lin et al., 1983)
Longwave radiation	RRTMG (Iacono et al., 2008)
Shortwave radiation	Goddard shortwave scheme (Chou and Suarez, 1994)
Surface Layer	MM5 Similarity based on Monin-Obukhov scheme (Beljaars, 1995)
Land-surface Physics	Noah Land Surface Model (Chen and Dudhia, 2001)
Urban surface physics	Urban Canopy Model (Kusaka and Kimura, 2004)
Planetary boundary layer	Yonsei University scheme (Hong et al., 2006)
Cumulus parametrization	Grell 3D scheme (Grell and Dévényi, 2002)

**Table 2.** Description of WRF-Chem simulations performed for this study.

Simulation Name	Model Chemistry	Photolysis Scheme
(1) MOZART	MOZART- 4 chemistry with gocart aerosols, KPP solver	Madronich F-TUV photolysis
(2) RADM2	RADM2 chemistry with MADE/SORGAM aerosols, KPP solver	Madronich photolysis (TUV)

**Table 3.** Observational datasets used for model evaluation.

Database	Parameter	Temporal Resolution	Data Source
BADC Global Weather Observation Data	MSLP, T2, WS10, WD10	3-hourly	<a href="http://badc.nerc.ac.uk/home/">http://badc.nerc.ac.uk/home/</a>
AirBase v7	O <sub>3</sub> , NO <sub>2</sub> , NO, NO <sub>x</sub>	hourly	<a href="http://www.eea.europa.eu/data-and-maps/data/airbase-the-european-air-quality-database-7">http://www.eea.europa.eu/data-and-maps/data/airbase-the-european-air-quality-database-7</a>
EMEP	NO <sub>2</sub> , NO, NO <sub>x</sub>	hourly	<a href="http://ebas.nilu.no/">http://ebas.nilu.no/</a>

**Table 4.** Domain-wide statistical performance of WRF-Chem against 3-hourly meteorological observations from BADC. Modeled quantities are from the MOZART simulation.

	Winter (DJF)							Spring (MAM)						
	Mean-Obs	Mean-Mod	MB	NMB	MFB	r	no. stations	Mean-Obs	Mean-Mod	MB	NMB	MFB	r	no. stations
MSLP (hPa)	1015.41	1014.79	-0.96	0.00	0.00	0.99	1297	1014.67	1014.46	-0.35	0.00	0.00	0.99	1295
T2 (° C)	2.51	2.99	0.29	0.11	-0.01	0.89	1581	9.73	9.91	-0.11	-0.01	0.07	0.94	1581
WS10 (m/s)	4.31	5.60	1.34	0.31	0.42	0.71	1577	3.86	4.46	0.65	0.17	0.29	0.68	1589
WD10 (deg)	175.53	203.73	27.93	0.16	0.27	0.50	1568	167.88	188.67	21.16	0.13	0.25	0.48	1580
	Summer (JJA)							Fall (SON)						
	Mean-Obs	Mean-Mod	MB	NMB	MFB	r	no. stations	Mean-Obs	Mean-Mod	MB	NMB	MFB	r	no. stations
MSLP (hPa)	1012.12	1012.11	0.04	0.00	0.00	0.98	1288	1017.61	1017.42	-0.49	0.00	0.00	0.99	1297
T2 (° C)	17.82	17.70	-0.38	-0.02	0.00	0.87	1573	9.20	9.65	0.24	0.03	-0.08	0.95	1583
WS10 (m/s)	3.45	3.90	0.48	0.14	0.27	0.63	1574	3.64	4.61	1.04	0.28	0.40	0.68	1585
WD10 (deg)	173.88	196.92	23.27	0.13	0.25	0.45	1561	172.30	196.49	24.02	0.14	0.27	0.48	1574

**Table 5.** Statistics for MOZART simulation against hourly observations from the AirBase network. Means and MB are expressed in  $\mu\text{g m}^{-3}$ ; NMB, MFB, and r are unitless. r is the hourly temporal correlation coefficient for all quantities except MDA8, for which it represents the daily temporal correlation coefficient.

	Winter (DJF)							Spring (MAM)						
	Mean-Obs	Mean-Mod	MB	NMB	MFB	r	no. stations	Mean-Obs	Mean-Mod	MB	NMB	MFB	r	no. stations
O <sub>3</sub>	53.82	48.34	-5.44	-0.10	-0.10	0.60	366	75.26	70.93	-4.25	-0.06	-0.07	0.56	371
MDA8	67.50	64.20	-3.30	-0.05	-0.04	0.76	365	96.33	97.00	0.67	0.01	0.00	0.69	370
NO <sub>x</sub>	20.22	16.99	-3.20	-0.16	0.00	0.37	204	14.30	13.32	-0.99	-0.07	-0.15	0.25	210
NO <sub>2</sub>	14.40	14.83	0.48	0.03	0.07	0.42	250	11.34	12.03	0.70	0.06	-0.10	0.30	252
NO	4.27	1.18	-3.10	-0.73	-1.24	0.29	148	2.65	0.79	-1.87	-0.70	-1.26	0.27	148
	Summer (JJA)							Fall (SON)						
	Mean-Obs	Mean-Mod	MB	NMB	MFB	r	no. stations	Mean-Obs	Mean-Mod	MB	NMB	MFB	r	no. stations
O <sub>3</sub>	70.84	80.72	9.92	0.14	0.14	0.55	370	47.24	53.10	6.14	0.13	0.13	0.57	367
MDA8	94.51	110.37	15.86	0.17	0.16	0.61	369	63.81	74.82	11.01	0.17	0.15	0.65	367
NO <sub>x</sub>	10.63	10.57	-0.10	-0.01	-0.21	0.16	206	19.14	16.62	-2.53	-0.13	-0.07	0.32	208
NO <sub>2</sub>	8.30	9.66	1.37	0.17	-0.12	0.22	248	13.60	15.23	1.64	0.12	0.05	0.38	253
NO	2.01	0.48	-1.53	-0.76	-1.36	0.19	148	4.24	1.07	-3.17	-0.75	-1.32	0.28	146

**Table 6.** Statistics for MOZART simulation against hourly observations from the EMEP network. Means and MB are expressed in  $\mu\text{g m}^{-3}$ ; NMB, MFB, and r are unitless. r is the hourly temporal correlation coefficient for all quantities except MDA8, for which it represents the daily temporal correlation coefficient.

	Winter (DJF)							Spring (MAM)						
	Mean-Obs	Mean-Mod	MB	NMB	MFB	r	no. stations	Mean-Obs	Mean-Mod	MB	NMB	MFB	r	no. stations
O <sub>3</sub>	54.54	43.82	-10.46	-0.19	-0.22	0.53	118	78.99	68.62	-10.53	-0.13	-0.16	0.55	120
MDA8	64.66	55.09	-9.57	-0.15	-0.16	0.56	117	95.64	90.15	-5.49	-0.06	-0.07	0.65	119
NO <sub>x</sub>	11.36	12.39	1.10	0.10	0.18	0.42	8	10.21	10.44	0.41	0.04	-0.04	0.33	9
NO <sub>2</sub>	10.19	13.24	3.09	0.30	0.25	0.53	34	8.07	10.72	2.55	0.32	-0.01	0.37	38
NO	2.10	1.22	-0.87	-0.41	-0.65	0.36	25	1.34	0.78	-0.56	-0.42	-0.50	0.35	27
	Summer (JJA)							Fall (SON)						
	Mean-Obs	Mean-Mod	MB	NMB	MFB	r	no. stations	Mean-Obs	Mean-Mod	MB	NMB	MFB	r	no. stations
O <sub>3</sub>	72.08	76.39	4.04	0.06	0.06	0.54	120	53.24	52.05	-1.08	-0.02	-0.02	0.54	122
MDA8	91.24	101.48	10.24	0.11	0.11	0.59	119	66.99	70.37	3.39	0.05	0.04	0.57	121
NO <sub>x</sub>	7.62	8.44	0.94	0.12	-0.12	0.30	9	11.83	12.14	0.76	0.06	0.03	0.34	9
NO <sub>2</sub>	6.07	9.10	2.96	0.49	0.06	0.30	38	8.88	13.81	5.08	0.57	0.23	0.40	38
NO	1.23	0.60	-0.64	-0.52	-0.52	0.28	29	1.42	1.23	-0.14	-0.10	-0.36	0.34	28

**Table 7.** Statistics for yearly SOMO35 in  $\text{mg m}^{-3} \cdot \text{days}$ .

Simulation	Observation network	Obs	Model	MB	NMB	MFB	no. stations
MOZART	AirBase	6.23	8.22	1.98	0.32	0.30	375
MOZART	EMEP	5.73	6.27	0.51	0.09	0.11	122
RADM2	AirBase	6.23	2.55	-3.68	-0.59	-0.87	375
RADM2	EMEP	5.73	1.84	-3.91	-0.68	-1.13	122



**Table 8.** Statistics for RADM2 simulation against hourly observations from the AirBase network. Means and MB are expressed in  $\mu\text{g m}^{-3}$ ; NMB, MFB, and r are unitless. r is the hourly temporal correlation coefficient for all quantities except MDA8, for which it represents the daily temporal correlation coefficient.

	Winter (DJF)							Spring (MAM)						
	Mean-Obs	Mean-Mod	MB	NMB	MFB	r	no. stations	Mean-Obs	Mean-Mod	MB	NMB	MFB	r	no. stations
O <sub>3</sub>	53.82	41.57	-12.18	-0.23	-0.25	0.60	366	75.26	53.36	-21.81	-0.29	-0.33	0.53	371
MDA8	67.50	56.04	-11.46	-0.17	-0.17	0.75	365	96.33	74.73	-21.60	-0.22	-0.25	0.67	370
NO <sub>x</sub>	20.22	13.75	-6.45	-0.32	-0.23	0.36	204	14.30	11.44	-2.87	-0.20	-0.32	0.21	210
NO <sub>2</sub>	14.40	11.90	-2.47	-0.17	-0.15	0.41	250	11.34	10.31	-1.01	-0.09	-0.27	0.27	252
NO	4.27	0.97	-3.31	-0.77	-1.34	0.27	148	2.65	0.67	-1.99	-0.75	-1.34	0.26	148
	Summer (JJA)							Fall (SON)						
	Mean-Obs	Mean-Mod	MB	NMB	MFB	r	no. stations	Mean-Obs	Mean-Mod	MB	NMB	MFB	r	no. stations
O <sub>3</sub>	70.84	57.79	-13.01	-0.18	-0.18	0.58	370	47.24	39.00	-8.03	-0.17	-0.18	0.59	367
MDA8	94.51	80.59	-13.92	-0.15	-0.15	0.71	369	63.81	56.02	-7.79	-0.12	-0.12	0.69	367
NO <sub>x</sub>	10.63	9.79	-0.87	-0.08	-0.29	0.14	206	19.14	14.30	-4.84	-0.25	-0.24	0.30	208
NO <sub>2</sub>	8.30	8.95	0.67	0.08	-0.19	0.21	248	13.60	12.57	-1.01	-0.07	-0.13	0.36	253
NO	2.01	0.46	-1.55	-0.77	-1.42	0.18	148	4.24	1.28	-2.97	-0.70	-1.27	0.26	146

**Table 9.** Statistics for RADM2 simulation against hourly observations from the EMEP network. Means and MB are expressed in  $\mu\text{g m}^{-3}$ ; NMB, MFB, and r are unitless. r is the hourly temporal correlation coefficient for all quantities except MDA8, for which it represents the daily temporal correlation coefficient.

	Winter (DJF)							Spring (MAM)						
	Mean-Obs	Mean-Mod	MB	NMB	MFB	r	no. stations	Mean-Obs	Mean-Mod	MB	NMB	MFB	r	no. stations
O <sub>3</sub>	54.54	38.67	-15.62	-0.29	-0.36	0.54	118	78.99	53.24	-25.83	-0.33	-0.40	0.49	120
MDA8	64.66	49.40	-15.26	-0.24	-0.27	0.56	117	95.64	71.04	-24.60	-0.26	-0.29	0.55	119
NO <sub>x</sub>	11.36	10.31	-0.99	-0.09	-0.02	0.38	8	10.21	8.76	-1.31	-0.13	-0.24	0.30	9
NO <sub>2</sub>	10.19	10.72	0.56	0.06	0.03	0.51	34	8.07	9.11	0.95	0.12	-0.19	0.34	38
NO	2.10	1.16	-0.93	-0.44	-0.67	0.37	25	1.34	0.68	-0.67	-0.50	-0.59	0.31	27
	Summer (JJA)							Fall (SON)						
	Mean-Obs	Mean-Mod	MB	NMB	MFB	r	no. stations	Mean-Obs	Mean-Mod	MB	NMB	MFB	r	no. stations
O <sub>3</sub>	72.08	55.65	-16.65	-0.23	-0.24	0.58	120	53.24	39.89	-13.21	-0.25	-0.29	0.57	122
MDA8	91.24	74.75	-16.49	-0.18	-0.19	0.69	119	66.99	54.31	-12.68	-0.19	-0.21	0.63	121
NO <sub>x</sub>	7.62	7.61	0.10	0.01	-0.24	0.28	9	11.83	10.59	-0.82	-0.07	-0.13	0.32	9
NO <sub>2</sub>	6.07	8.33	2.20	0.36	-0.02	0.29	38	8.88	11.48	2.71	0.31	0.04	0.39	38
NO	1.23	0.52	-0.73	-0.59	-0.58	0.25	29	1.42	1.43	0.07	0.05	-0.31	0.31	28

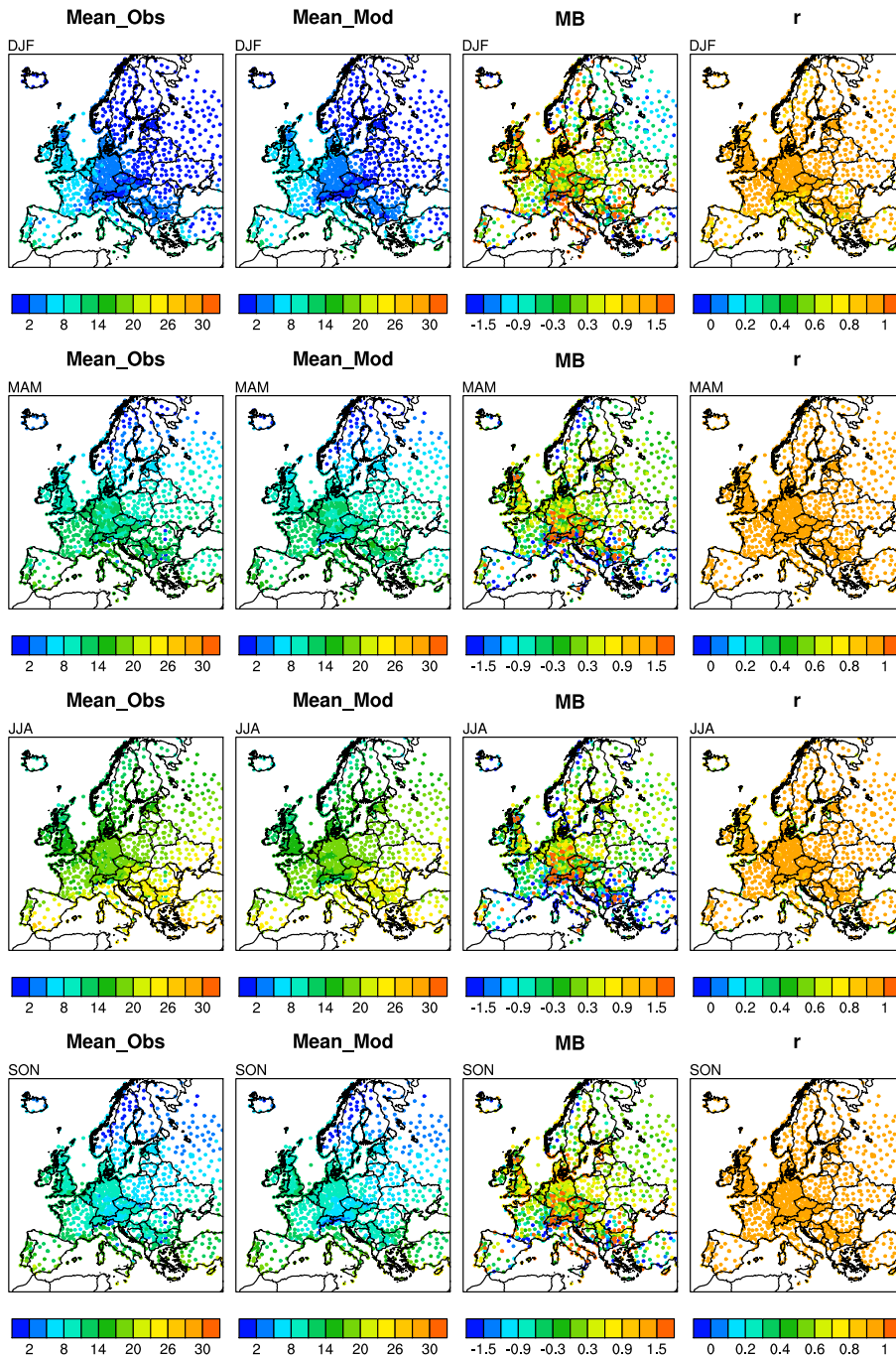


**Figure 1.** Seasonal average values of 2-meter temperature (T2) in degrees Celcius. Model results and statistics are shown for the MOZART simulation at the locations of the observations.

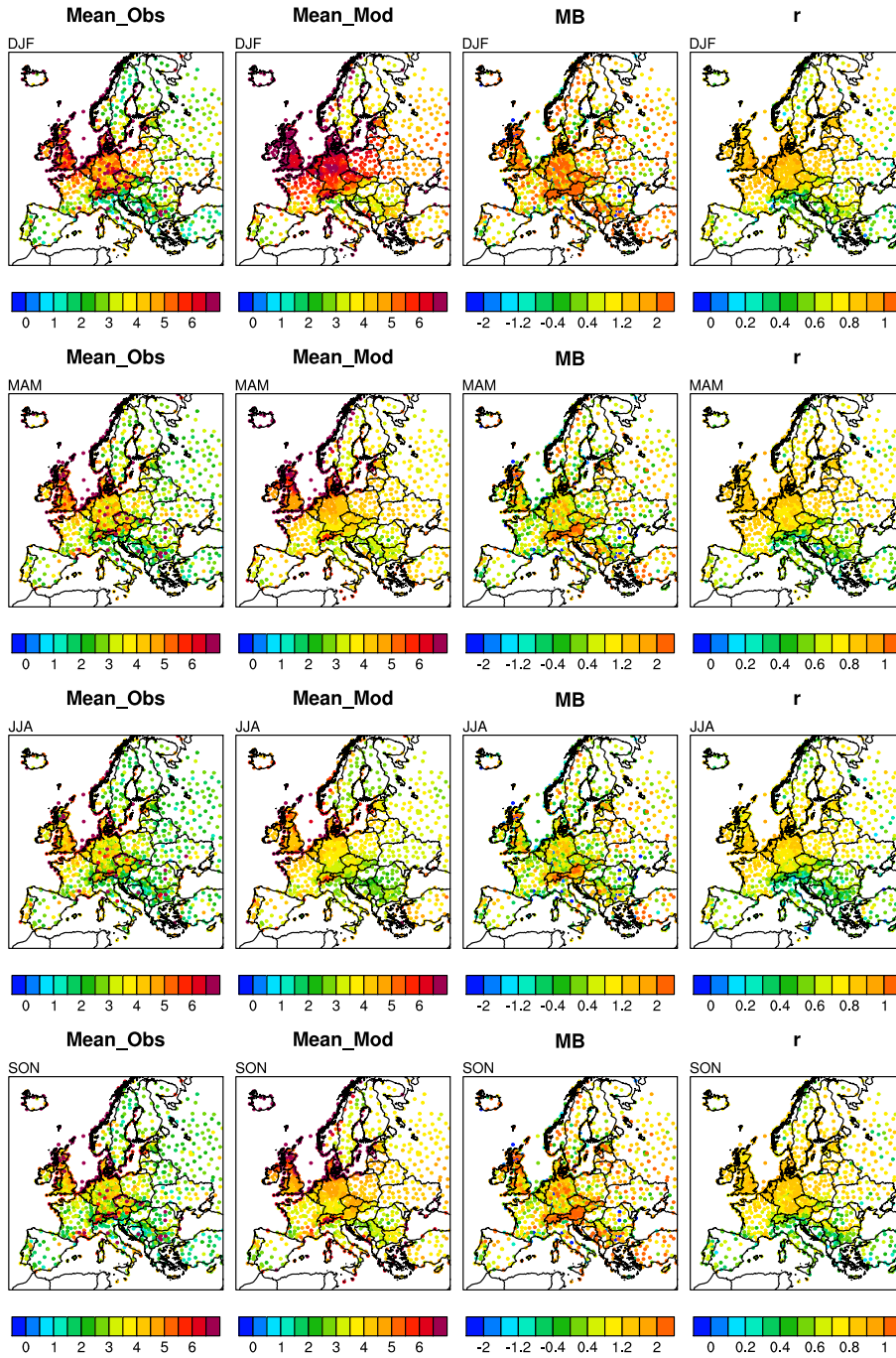


**Figure 2.** Seasonal average values of 10-meter wind speed (WS10) in m/s. Model results and statistics are shown for the MOZART simulation at the locations of the observations.

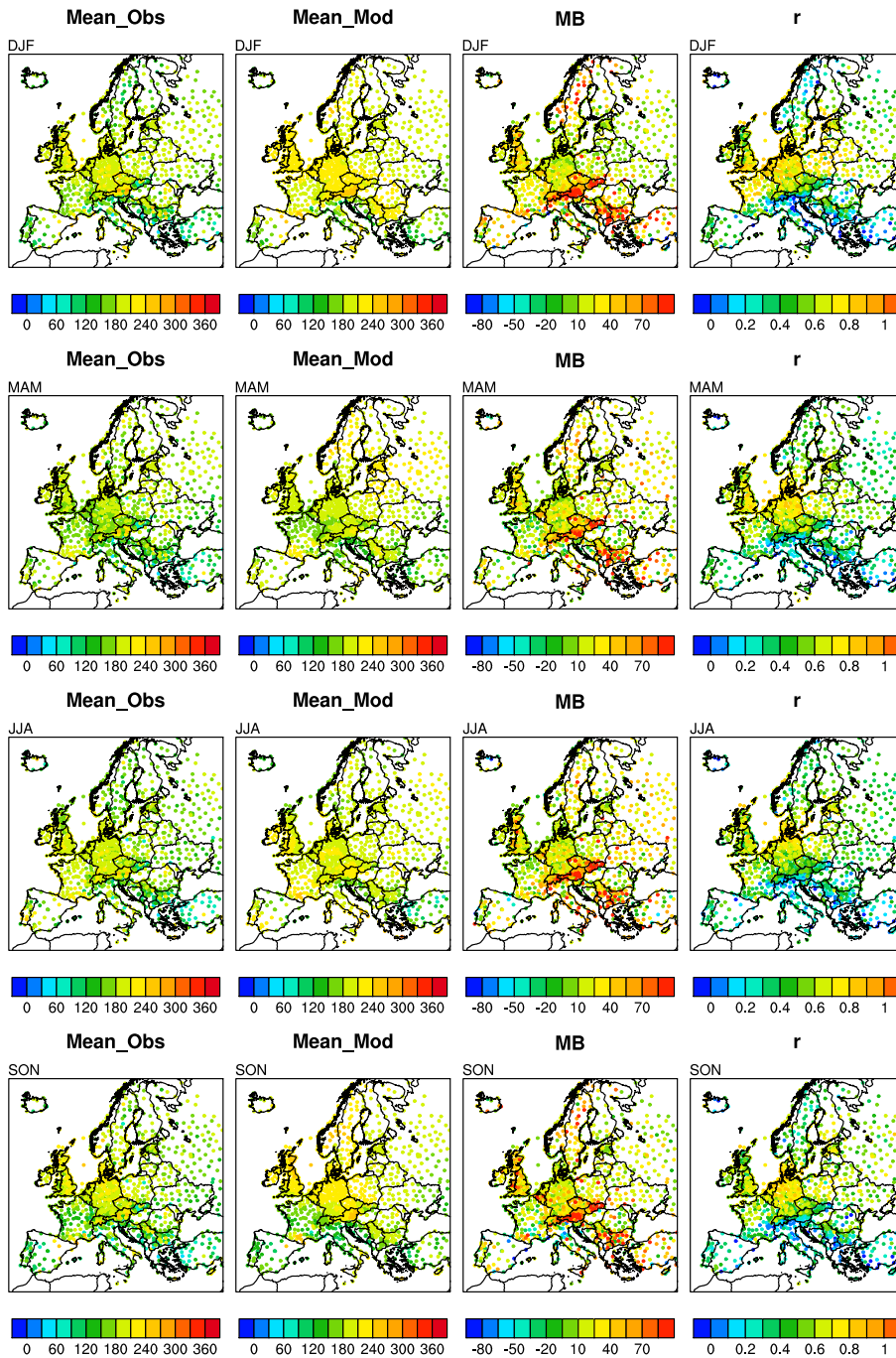


**Figure 3.** Seasonal average values of 10-meter wind direction (WD10) in degrees. Model results and statistics are shown for the MOZART simulation at the locations of the observations.

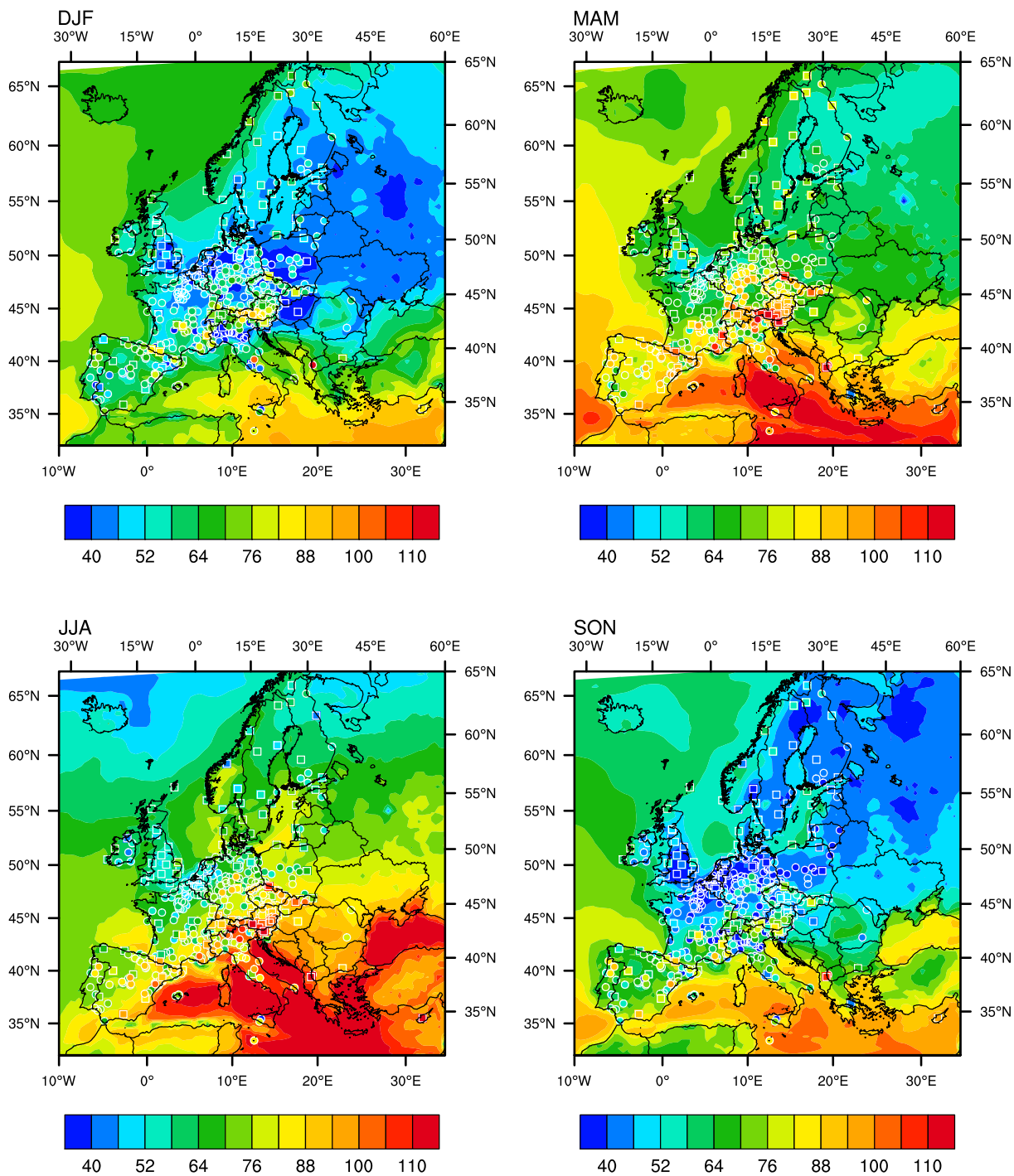


**Figure 4.** Seasonal average values of surface  $O_3$  in  $\mu\text{g m}^{-3}$ . Contours are model output from the MOZART simulation. Filled dots represent hourly measurements at AirBase rural background stations, filled squares represent measurements at EMEP stations.



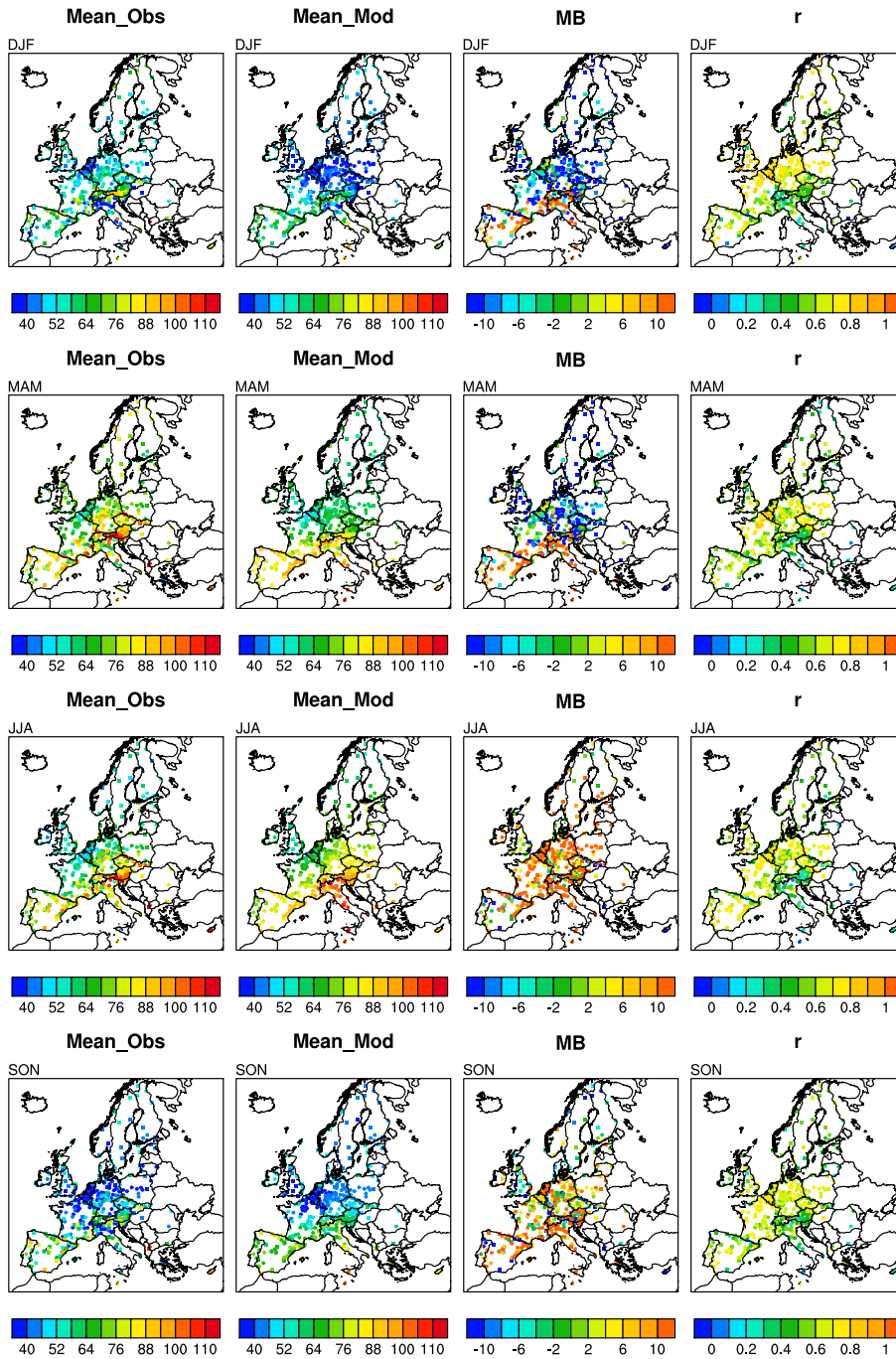


**Figure 5.** Seasonal average values of surface  $O_3$  in  $\mu\text{g m}^{-3}$  from hourly measurements at AirBase (circles) and EMEP (squares) stations, and modeled values from MOZART for corresponding locations. The Mean Bias (MB, in  $\mu\text{g m}^{-3}$ ) and temporal correlation coefficient ( $r$ ) for hourly values are also shown at the location of station observations.

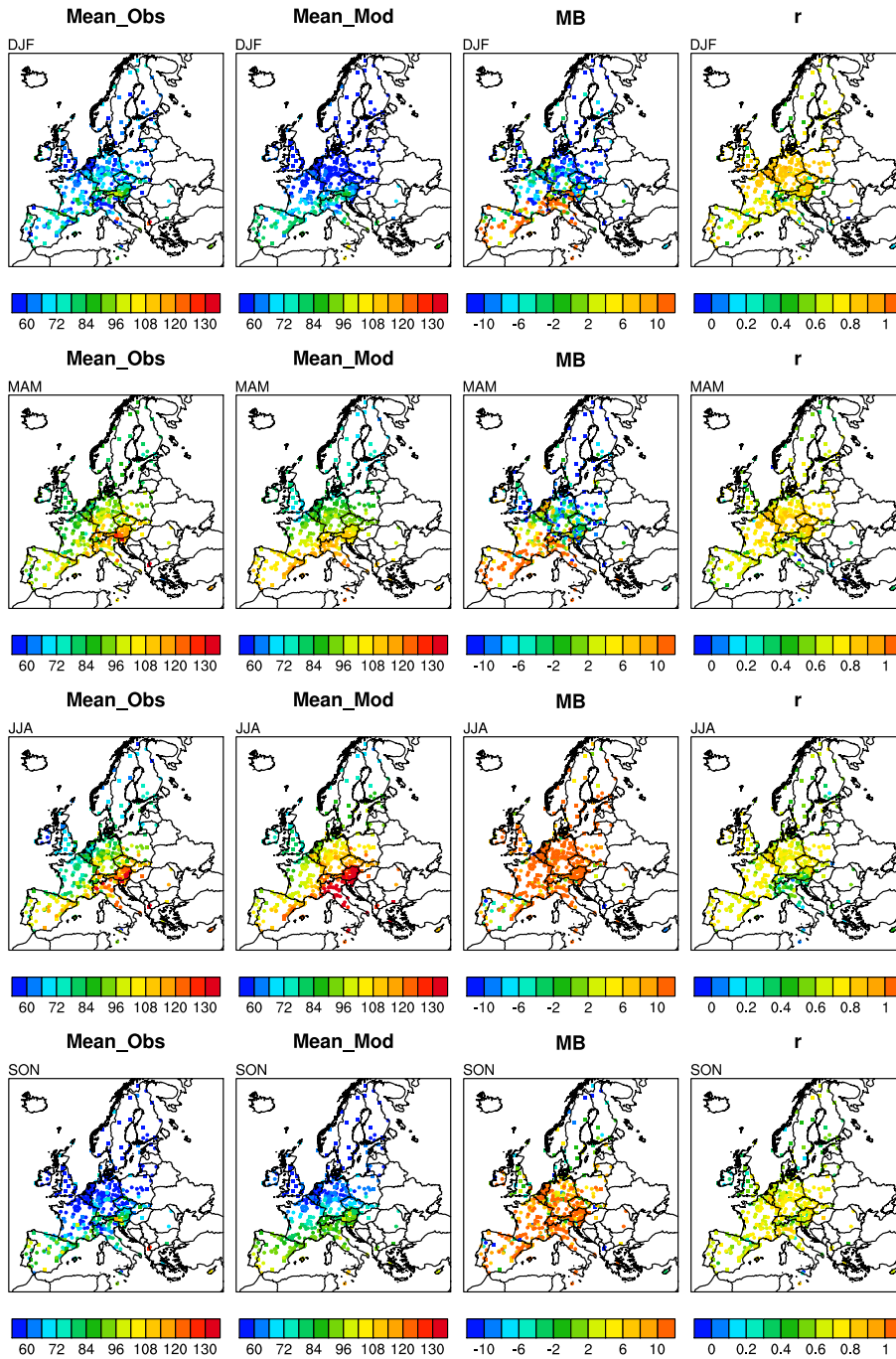


**Figure 6.** Seasonal average values of MDA8 in  $\mu\text{g m}^{-3}$  calculated from hourly measurements at AirBase (circles) and EMEP (squares) stations, and modeled values from MOZART for corresponding locations. The Mean Bias (MB, in  $\mu\text{g m}^{-3}$ ) and temporal correlation coefficient (r) for daily values are also shown at the location of station observations.



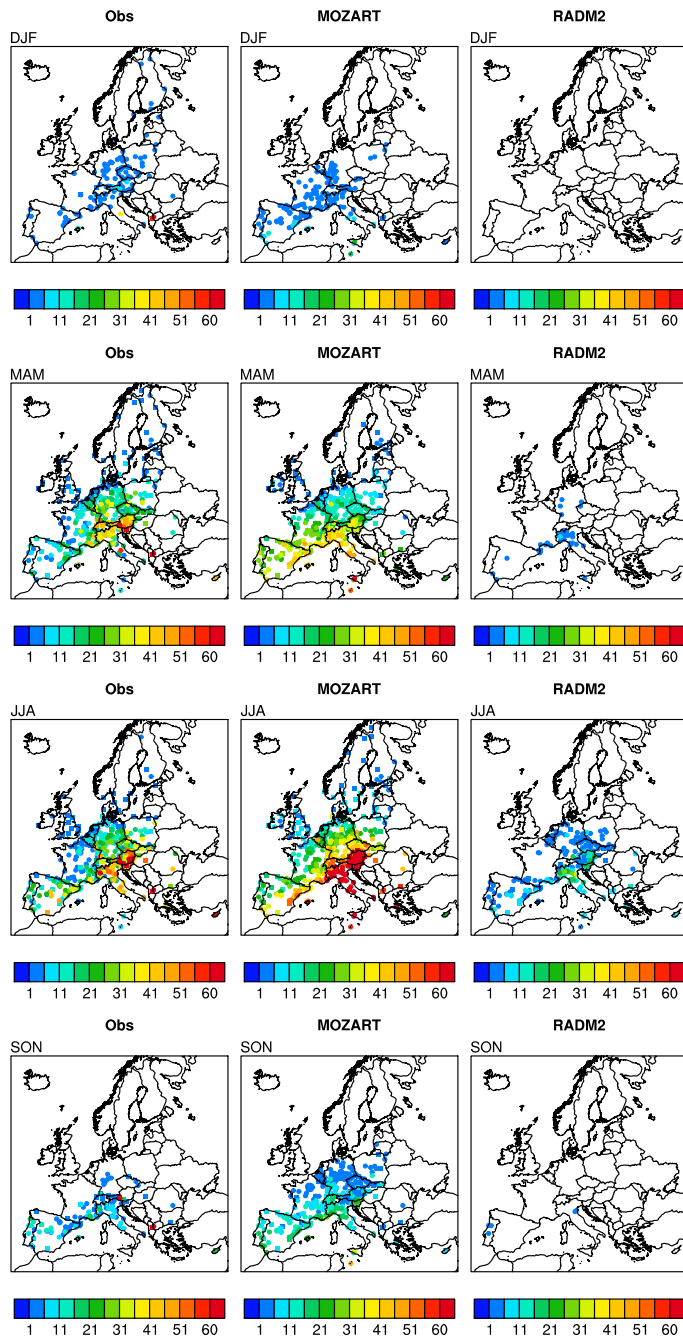


**Figure 7.** Number of days of exceedances of the EU long-term objective value for MDA8 ( $120 \mu\text{g m}^{-3}$ ) at AirBase (circles) and EMEP (squares) station locations. Shown are totals by season for observations and the MOZART and RADM2 simulations. For simplicity of viewing the data, stations with no exceedances are not plotted.

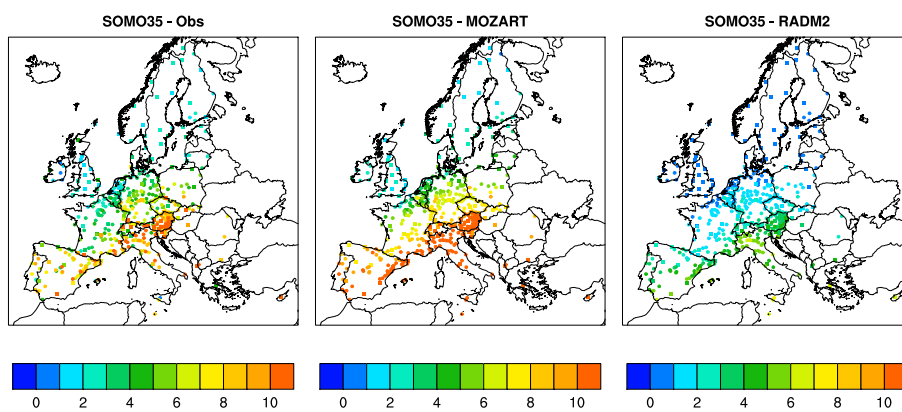


**Figure 8.** Yearly values of SOMO35 in  $\text{mg m}^{-3} \cdot \text{days}$  calculated from hourly measurements at AirBase (circles) and EMEP (squares) stations, and modeled values for corresponding locations.

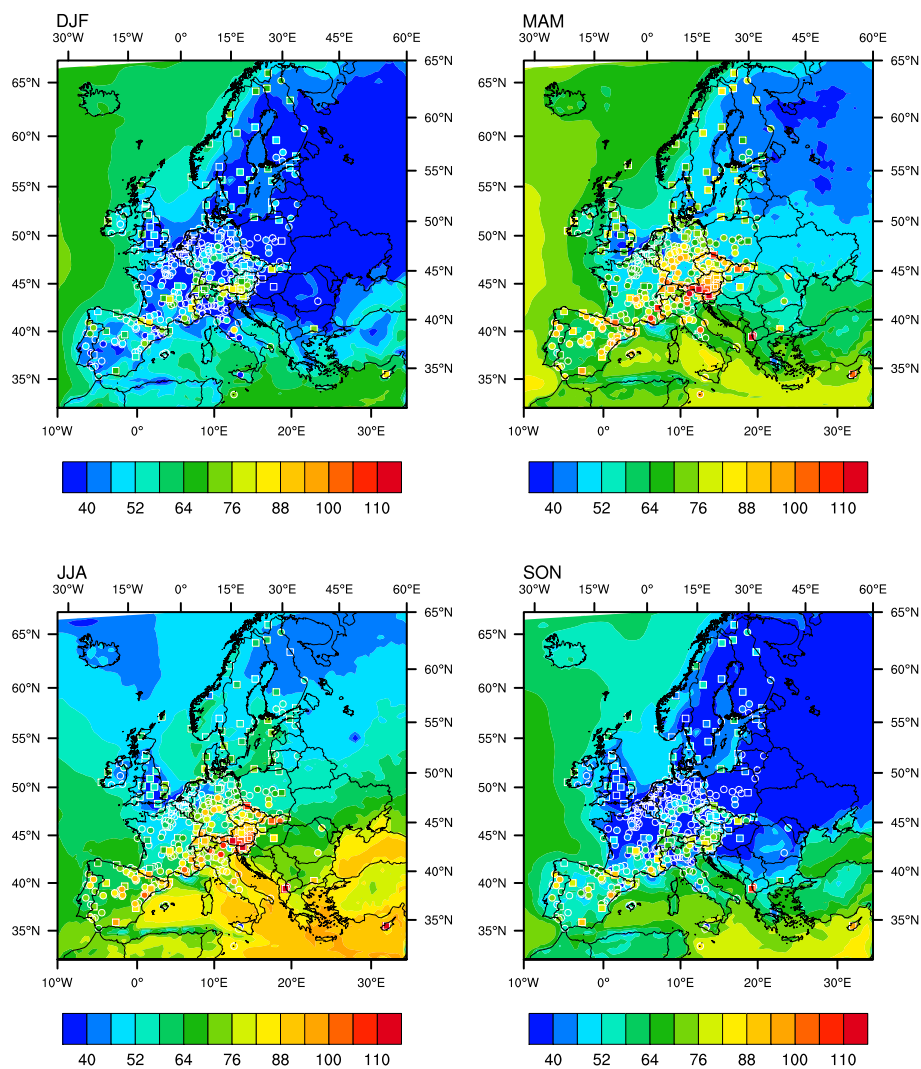


**Figure 9.** Seasonal average values of surface O<sub>3</sub> in µg m<sup>-3</sup>. Contours are model output from the RADM2 simulation. Filled dots represent hourly measurements at AirBase rural background stations, filled squares represent measurements at EMEP stations.

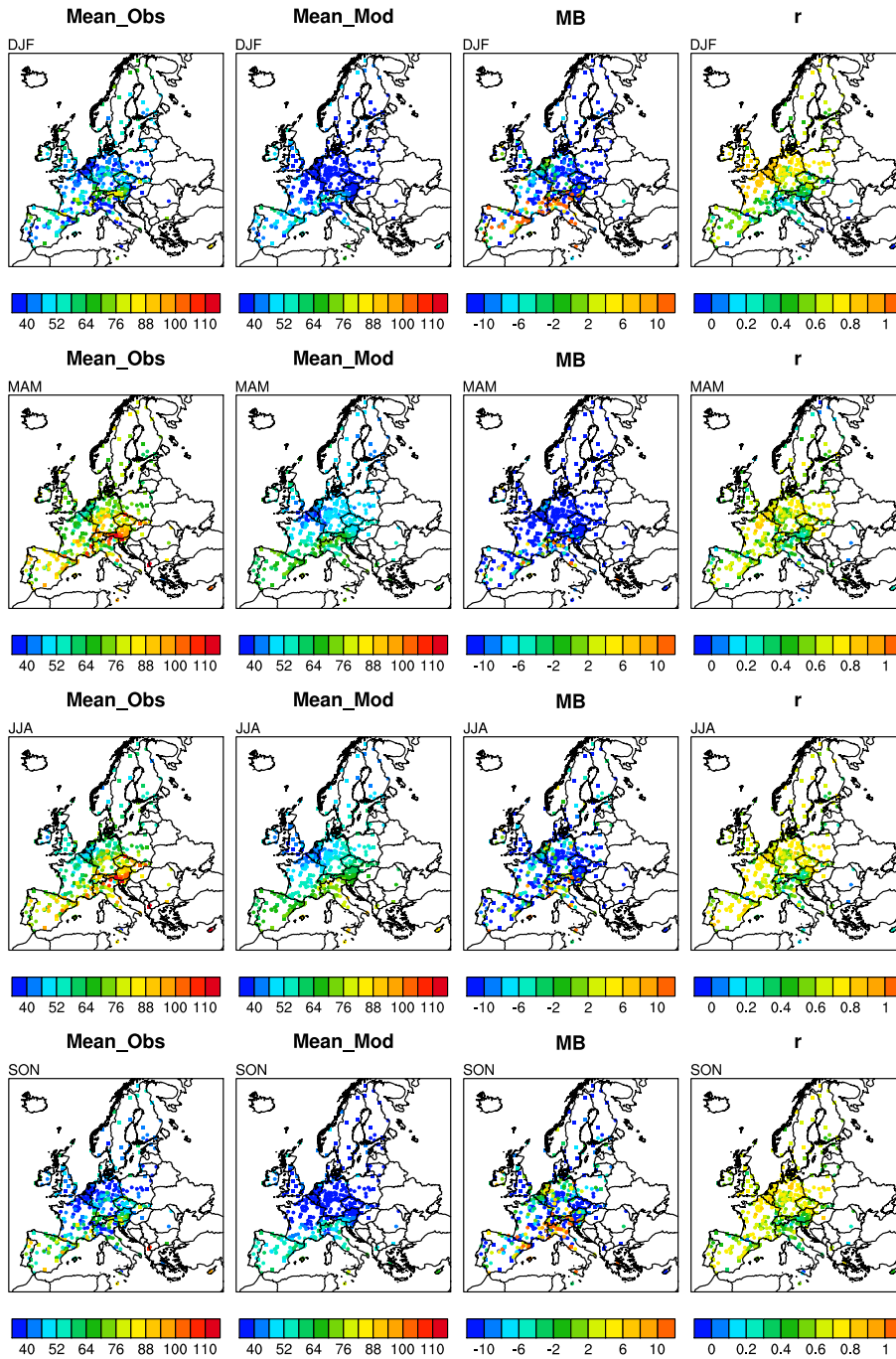


**Figure 10.** Seasonal average values of surface  $O_3$  in  $\mu g m^{-3}$  from hourly measurements at AirBase (circles) and EMEP (squares) stations, and modeled values from RADM2 for corresponding locations. The Mean Bias (MB, in  $\mu g m^{-3}$ ) and temporal correlation coefficient (r) for hourly values are also shown at the location of station observations.

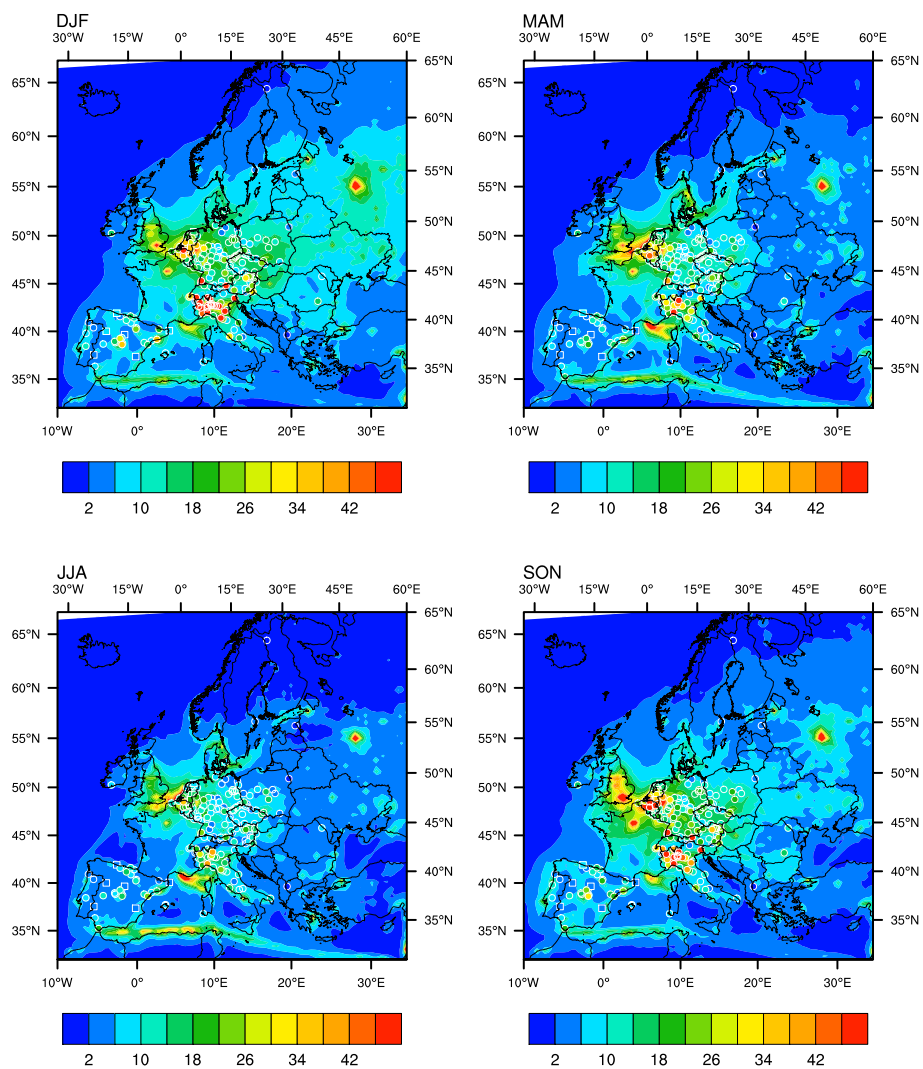


**Figure 11.** Seasonal average values of surface NO<sub>x</sub> in µg m<sup>-3</sup>. Contours are model output from the MOZART simulation. Filled dots represent hourly measurements at AirBase rural background stations, filled squares represent measurements at EMEP stations.

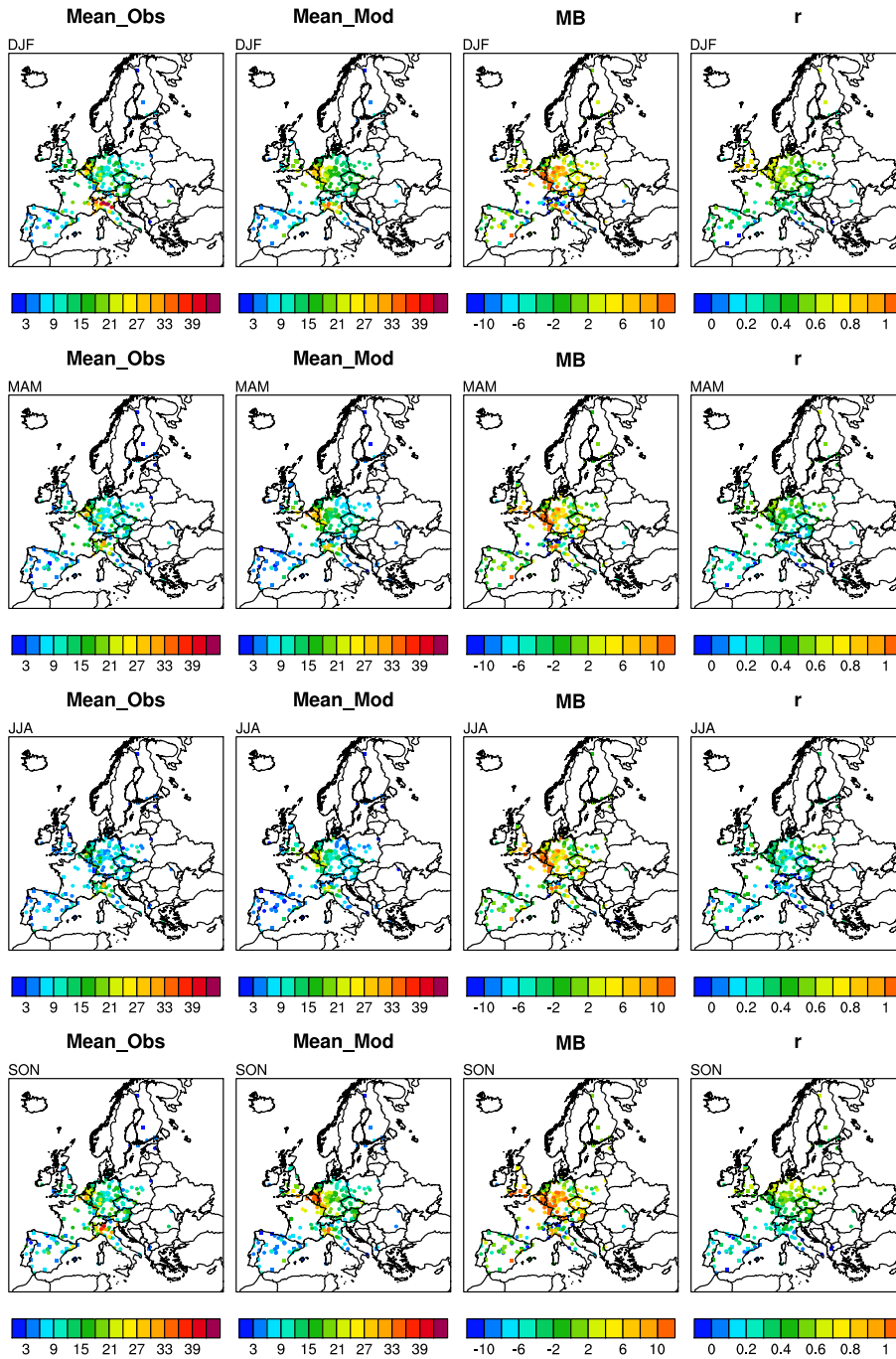


**Figure 12.** Seasonal average values of surface  $\text{NO}_2$  in  $\mu\text{g m}^{-3}$  from hourly measurements at AirBase (circles) and EMEP (squares) stations, and modeled values from MOZART for corresponding locations. The Mean Bias (MB) and temporal correlation coefficient ( $r$ ) for hourly values are also shown at the location of station observations.

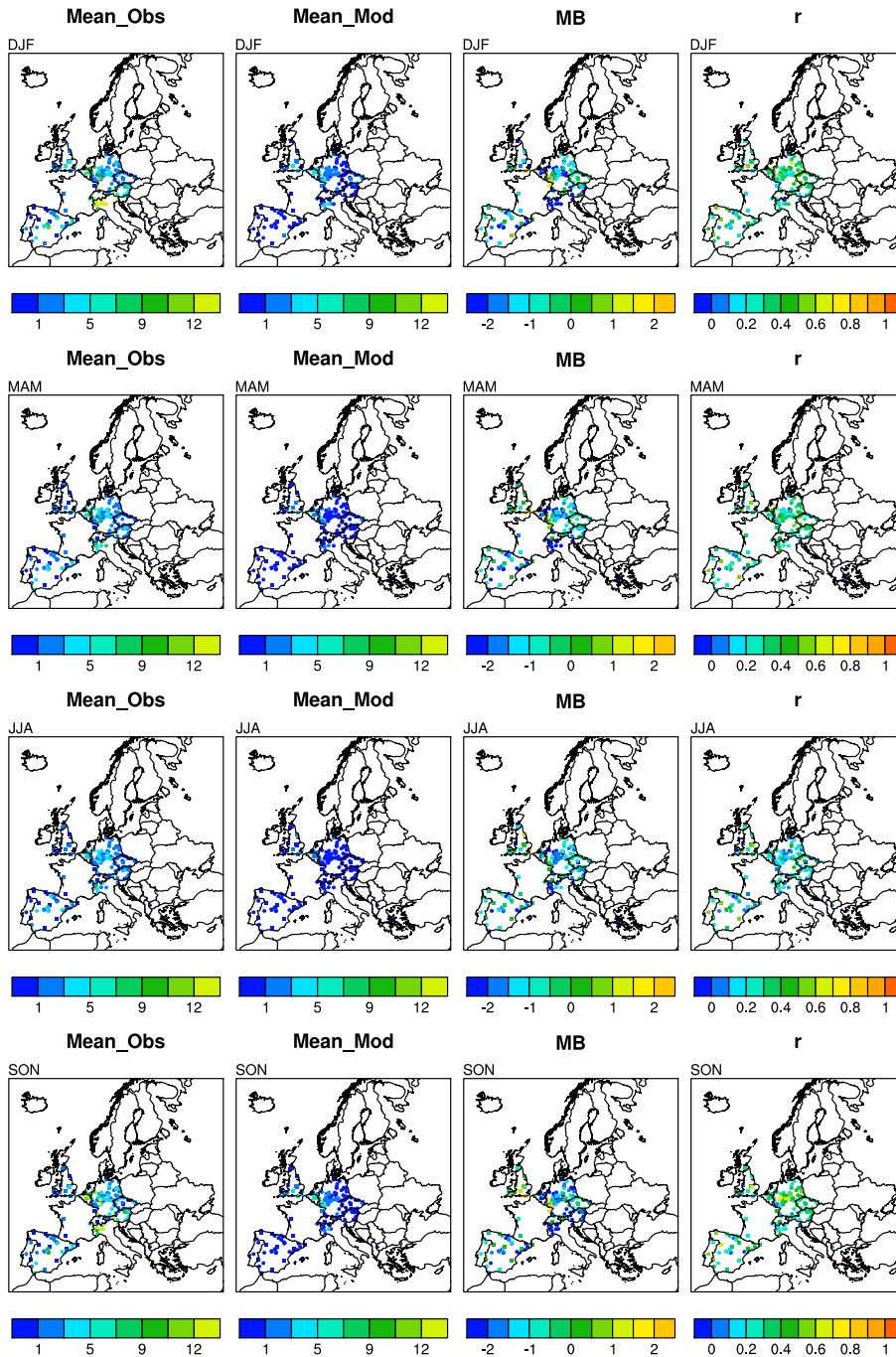


**Figure 13.** Seasonal average values of surface NO in  $\mu\text{g m}^{-3}$  from hourly measurements at AirBase (circles) and EMEP (squares) stations, and modeled values from MOZART for corresponding locations. The Mean Bias (MB) and temporal correlation coefficient (r) for hourly values are also shown at the location of station observations.



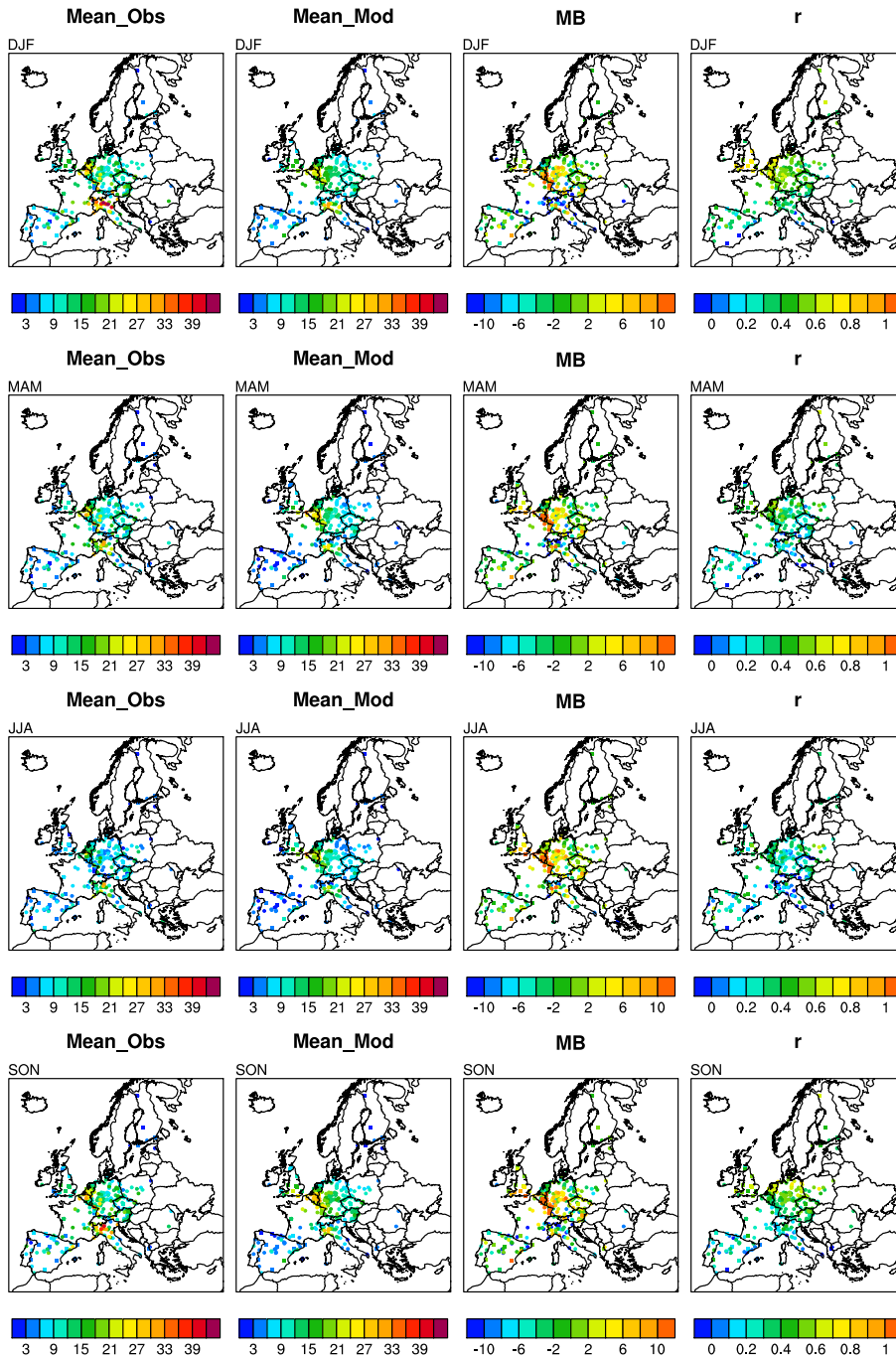


**Figure 14.** Seasonal average values of surface  $\text{NO}_2$  in  $\mu\text{g m}^{-3}$  from hourly measurements at AirBase (circles) and EMEP (squares) stations, and modeled values from RADM2 for corresponding locations. The Mean Bias (MB) and temporal correlation coefficient ( $r$ ) for hourly values are also shown at the location of station observations.



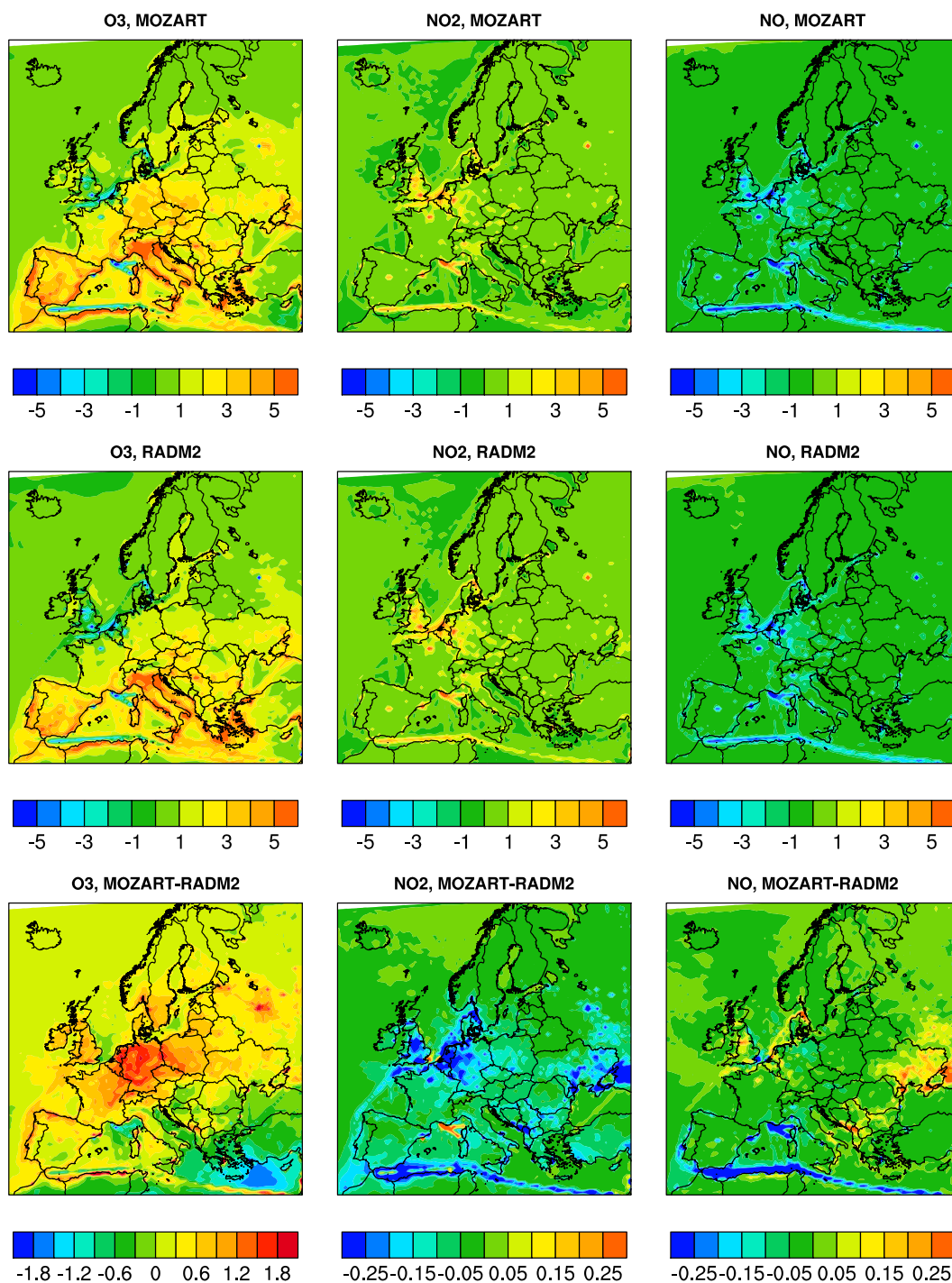


**Figure 15.** Net midday (11:00 - 14:00 CEST) photochemical production rate in ppb hr<sup>-1</sup> for O<sub>3</sub>, NO<sub>2</sub>, and NO shown for MOZART and RADM2 for July 2007. The last row shows the difference in net production rate in ppb hr<sup>-1</sup> (RADM2 subtracted from MOZART).

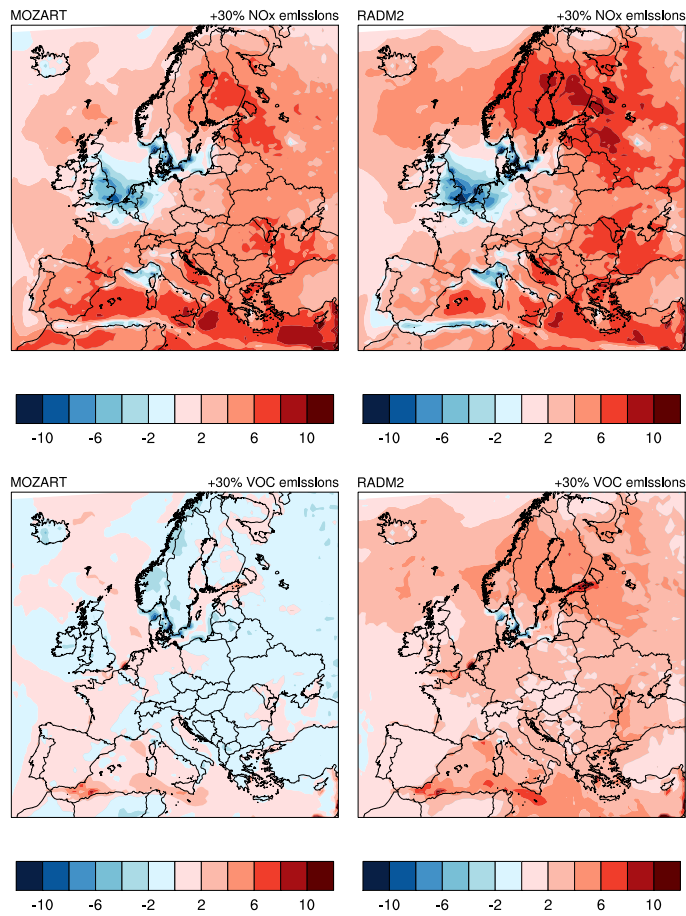


**Figure 16.** Sensitivity of average O<sub>3</sub> for July 2007 to a 30% increase in emissions of NO<sub>x</sub> (upper row) or VOC (lower row), shown for the MOZART and RADM2 chemical mechanisms. Shown here is the percent change in O<sub>3</sub> concentration, i.e.,  $100 \times ([O_3]_{+30\% \text{ emissions}} - [O_3]_{\text{base}}) / [O_3]_{\text{base}}$ .